Original Article

MOLECULAR METABOLISM

Pde5a deficiency prevents diet-induced obesity via adipose cAMP-PKA activation enhancing fat browning

Federica Campolo[1,2,3,*], Ottavia Giampaoli[4,5], Federica Barbagallo[6], Biagio Palmisano[7], Anna Di Maio[8], Francesca Sciarra[1], Flavio Rizzo[1], Serena Monti[9], Sandra Albanese[9], Silvia Cardarelli[10], Maria Rita Assenza[6], Eleonora Poggiogalle[1], Adriano Patriarca[11], Fabio Sciubba[4,5], Antonio Filippini[2], Andrea Lenzi[1], Daniele Gianfrilli[1], Mauro Giorgi[10], Susanna Dolci[12], Fabio Naro[2], Maurilio Sampaolesi[2], Mara Riminucci[6], Alfredo Miccheli[4], Lino Tessarollo[13], Mary Anna Venneri[1], Andrea M. Isidori[1,]**

ABSTRACT

Objective: Cyclic nucleotides are central regulators of adipogenesis and adaptive thermogenesis, with their intracellular concentrations tightly controlled by phosphodiesterases (PDEs). Among them, phosphodiesterase type 5 (PDE5A) regulates cyclic guanosine monophosphate (cGMP) turnover in adipocytes. Although PDE5A inhibition has been explored in diabetes, its role in systemic metabolism remains poorly defined.
Methods: We employed different *Pde5a* knockout mouse models to investigate the impact of PDE5A deficiency on adipose tissue biology and whole-body energy homeostasis. Phenotypic, histological, and metabolic assessments were performed under chow and high-fat diet conditions, with a focus on thermogenic activation, hepatic lipid accumulation, and glucose metabolism.
Results: Loss of *Pde5a* resulted in robust activation of brown adipose tissue and moderate browning of white adipose depots, accompanied by a reduction in hepatic lipid content. Upon high-fat diet challenge, *Pde5a*-deficient mice exhibited resistance to obesity, improved glucose handling, and enhanced thermogenic capacity. Mechanistically, these protective effects originated from early developmental knockdown of *Pde5a*, which induced metabolic reprogramming via activation of the cAMP—protein kinase A (PKA) signaling pathway. The convergence of cGMP and cAMP signaling cascades orchestrated systemic metabolic adaptations.
Conclusions: Our study identifies PDE5A as a previously unrecognized regulator of thermogenesis and energy balance. Targeting PDE5A may therefore represent a promising adjuvant therapeutic approach for the treatment of metabolic disorders.

Keywords Phosphodiesterases; cGMP; PDE5i; Obesity; Browning; Lipid metabolism

1. INTRODUCTION

Adipose tissue (AT) has long been recognized as the principal site of energy storage, playing a critical role in whole-body energy homeostasis [1]. However, recent advances have transformed our understanding of AT, revealing it to be a dynamic endocrine organ composed of a heterogeneous population of cells including mature and immature adipocytes, immune cells, endothelial cells, progenitor and stem cells that collectively orchestrate complex metabolic responses. Dysregulation in the composition and function or excessive expansion of adipose tissue drives the complications observed in obesity and related conditions [2]. As the global prevalence of morbid

[1]Department of Experimental Medicine, Sapienza University of Rome, Rome, 00161, Italy [2]Department of Anatomy, Histology, Forensic Medicine and Orthopedics, Unit of Histology and Medical Embryology, Sapienza University of Rome, Rome, 00161, Italy [3]Saint Camillus International, University of Health Sciences, Rome, 00133, Italy [4]NMR-Based Metabolomics Laboratory (NMLab), Sapienza University of Rome, Rome, 00185, Italy [5]Department of Environmental Biology, Sapienza University of Rome, Rome, 00185, Italy [6]Faculty of Medicine and Surgery, "Kore" University of Enna, Enna, 94100, Italy [7]Department of Molecular Medicine, Sapienza University of Rome, Rome, 00161, Italy [8]CEINGE Biotecnologie Avanzate Franco Salvatore, Naples, 80145, Italy [9]National Research Council, Institute of Biostructures and Bioimaging, Naples, 80145, Italy [10]Department of Biology and Biotechnology "C. Darwin", Sapienza University of Rome, Rome, 00185, Italy [11]Department of Chemistry, Sapienza University of Rome, Rome, 00185, Italy [12]Department of Biomedicine and Prevention, University of Rome Tor Vergata, Rome, 00133, Italy [13]Mouse Cancer Genetics Program, Center for Cancer Research, National Cancer Institute, National Institutes of Health, Frederick, MD, USA

*Corresponding author. Department of Experimental Medicine, Sapienza University of Rome, Viale Regina Elena 324, 00161, Rome, Italy. E-mail: federica.campolo@uniroma1.it (F. Campolo).

**Corresponding author. Department of Experimental Medicine, Sapienza University of Rome, Viale Regina Elena 324, 00161, Rome, Italy. E-mail: andrea.isidori@uniroma1.it (A.M. Isidori).

Received April 22, 2025 • Revision received August 25, 2025 • Accepted August 26, 2025 • Available online 3 September 2025

https://doi.org/10.1016/j.molmet.2025.102243

obesity and metabolic-associated fatty liver disease (MAFLD) continue to rise [3], the need to identify novel molecular targets and pathways governing energy metabolism becomes ever more urgent. One promising but underexplored avenue is the pharmacological modulation of cyclic nucleotide signaling through the inhibition of phosphodiesterases (PDEs), enzymes responsible for the hydrolysis of cyclic nucleotides. Among these, phosphodiesterase 5 PDE5A stands out as the most extensively studied and clinically relevant, owing to the availability of human safe and affordable inhibitors. PDE5A selectively hydrolyzes cGMP [4], and its pharmacological inhibition has been shown to induce uncoupling protein 1 (UCP1) expression, promote thermogenic activity, and stimulate the browning of subcutaneous white adipose tissue [5,6]. Additionally, PDE5A inhibition has been implicated in adipogenesis, as evidenced by increased intracellular lipid droplet accumulation and the upregulation of key adipogenic markers during 3T3-L1 preadipocyte differentiation [7]. Preclinical and clinical studies seem to suggest that PDE5A inhibitors (PDE5i) improve insulin resistance and glucose metabolism highlighting their therapeutic potential for metabolic disorders [8—10]. We have extensively tested PDE5i in type 2 diabetes mellitus (T2DM) [11—15]; however, the precise mechanisms underlying these effects remains poorly understood. Building on these findings, we aim to dissect the specific contributions of PDE5A in the regulation of glucose homeostasis and lipid metabolism. To achieve this purpose, we developed constitutive and conditional *Pde5a* knockout mouse models and we investigated their metabolic phenotype, fat distribution and functional properties under basal conditions and following thermogenic and dietary challenges.

2. MATERIALS AND METHODS

2.1. Mice

Pde5a$^{-/-}$ mice were generated using CrispR-Cas9 technology according to the strategy depicted in Figure S1A. sgRNAs for targeting murine *Pde5a* exon 2 were designed using the online tool MIT CRISPR Design (http://news.mit.edu/). Guide RNAs were generated in vitro using the MEGAshortscript T7 transcription Kit (Thermo Fisher Scientific, MA, USA) and purified by using the MEGAclear Transcription Clean-Up Kit (Thermo Fisher Scientific, MA, USA). sgRNA (50 ng/μl), ssDNA donor oligo (100 ng/μl) and Cas9 mRNA (100 ng/μl; TriLink Biotechnologies, CA, USA) were microinjected into one-cell-stage zygotes obtained from C57BL/6N mice for the generation of *Pde5a* KO mice. C57BL/6N-B6D2F1/J chimeric mice were backcrossed to obtain a pure C57BL/6N background. Three founder lines were obtained and used for characterization.

Pde5a conditional knockout mice (*Pde5a*$^{LoxP/LoxP}$) were generated using homologous recombination and BAC technologies according to the strategy depicted in Figure S1B. BAC RP23-255K12 (Source BioScience Life Sciences), which consists of a 190 kb insert, including 100 kb of sequence upstream of the *Pde5a* start codon and 90 kb of mouse *Pde5a* gene, was used to generate targeting vector. Bacteria containing BAC RP23-255K12 were electroporated with mini-λ prophage DNA containing the essential components for homologous recombination. Targeting vector was generated by homologous recombination inserting the neomycin cassette, obtained from the pLTM260 vector (a generous gift of Dr. S.K. Sharan, NCI- FCRF, Frederick, MD) flanked by *LoxP* and *FRT* sites and two homology regions of the *Pde5a* gene at intron 2, into the BAC. A third *LoxP* site was introduced at intron 1. Kanamycin resistant recombinants were used for getting the BAC sequence (from intron 1 to intron 2) and the Neo cassette into the retrieval pDTa8 vector (a generous gift of Dr. S.K. Sharan, NCI- FCRF, Frederick, MD) containing the DT (diphtheria toxin) gene for negative selection of electroporated ES (embryonic stem cells). Targeting vector was linearized with NotI and electroporated into 129/Sv-C57BL/6N ES cells. Positive selection of recombinant clones was achieved using 200 μg/ml G418 (Thermo Fisher Scientific, MA, USA). 384 resistant clones were obtained and screening by Southern Blotting using two external 5′ and 3′ probes (SpeI) and an internal probe (PvuII). An ES targeted clone was injected into C57BL/6N blastocysts and finally returned to pseudopregnant CD1 mothers to produce germ-line chimeric pups. Neomycin cassette was removed crossing homozygous mice with Flp-C57BL/6N deleter mice (kindly provided by Prof. D. O'Carroll, EMBL Monterotondo, Italy). AdipoQ^{Cre} and Fabp4^{Cre} mice were kindly provided by Prof. M. Riminucci (Sapienza University of Rome, Italy) while Rosa26^{CreERT} were kindly provided by Prof. S. Dolci (University of Rome Tor Vergata, Italy).

Pde5a$^{-/-}$ mice genotyping was performed using the Phire Tissue Direct PCR Master Mix (Thermo Fisher Scientific, MA, USA) and following primers: *Pde5a* screen F1: 5′- GAGTCTAGGATAGGAGCACT -3′′, *Pde5a* screen F2: 5′- TTGGCAAGGAATGTGGCTA -3′ and *Pde5a* screen R: 5′- GCAGGCTTGTTATTTACTTATTTTG -3′. Pde5$^{LoxP/LoxP}$ mice genotyping was performed using the same Master Mix and the following primers: *Pde5a* del F: 5′-CCAGGTCATGAGAATGCACA and *Pde5a* del R: 5′- TGTCTCTTGGACTGGCAGA. All mice used for experiments were provided with food and water ad libitum and kept in a standard specific pathogen-free environment. The study focused on male mice as hormonal fluctuations associated with estrous cycle in females could influence glucose and lipid metabolism [16].

All procedures were conducted in compliance with the Guidelines for Animal Care and Treatment of the European Union and Italian Law (D. Lgs 2010/63EU) and were approved by the Sapienza University's Animal Research Ethics Committee, the Italian Ministry of Health and the Committee of Animal Care and Use of the National Cancer Institute in Frederick, Maryland (Authorization no. 165/2016-PR). The study conformed to Animal Research Reporting of In Vivo Experiments (ARRIVE) guidelines.

2.2. High-fat diet feeding protocol

A diet induced obesity (DIO) model was established through chronic feeding with a HFD (60 % kcal from fat, D12492, Research Diets, NJ, USA) for 12 weeks starting at the age of 8 weeks. Normal chow diet-fed mice were maintained on diet with 10 % kcal from fat (D12450J, Research Diets, NJ, USA). Food and water were provided ad libitum. Mice were housed and kept on a 12 h light/dark cycle at 23 ± 1 °C and weighed before HFD induction and once a week for all the duration of HFD feeding protocol. Food and water intake was determined weekly for all the duration of the experiment. Food Efficiency Ratio (FER) was calculated as: FER = 100*(weight/food intake) as previously described [17].

2.3. In vivo thermogenesis induction

For cold-induced thermogenesis 8-week-old male mice (n = 5/group) were housed at a constant room temperature of 4 °C for 4h according to [18]. For chemically induced thermogenesis 8-week-old male mice (n = 6/group) were injected via *ip* with 1 mg/kg β3 adrenoceptor agonist CL316,243 (Sigma-Aldrich, MA, USA) or saline for 10d as previously described [19]. Mice were weighted before and at the end of the treatment. Mice were housed at a constant room temperature

of 23 ± 1 °C with food and water given ad libitum and were fed a standard diet that contains 62 % kcal from carbohydrate, 25 % kcal from protein, and 13 % kcal from fat (Inotiv, IL, USA).

2.4. Statistics

All experiments were conducted with biological replicates or triplicates and confirmed with technical triplicates. Data are presented as mean ± SEM from at least three independent experiments. Full details for statistics are detailed within each material and methods paragraph. Data distribution was assumed to be normal but this was not formally tested. Statistical significance was analyzed using the student's t-test for parametric data and the ANOVA test with Tukey's corrections for nonparametric data. All differences were considered statistically significant when *p < 0.05, **p < 0.01, ***p < 0.005 and ****p < 0.001. All analyses were performed using GraphPad Prism 9 software.

3. RESULTS

3.1. Pde5a ablation boosts browning of WAT and thermogenic capacity

The protein kinase G (PKG) signaling pathway plays a crucial role in brown adipocyte differentiation, with several evidences demonstrating that pharmacological enhancement of cGMP in adipocytes induce UCP1 expression and drive the thermogenic program [5,6,20]. cGMP intracellular levels are primarily regulated by the *Pde5a* and *Pde9a* isoenzymes, both of which are expressed in mature adipocytes [9,21,22]. While recent evidence has shown that *Pde9a* is involved in the cold-induced thermogenic program of brown adipose tissue (BAT) [22], the role of *Pde5a* in this process warrants further investigation. To determine whether PDE5A contributed to white adipose tissue (WAT) browning and thermogenesis, we generated a *Pde5a* knockout (KO) mouse model (*Pde5a*$^{-/-}$) (Figure S1A and B) and analyzed its adipose tissue under basal conditions and after thermogenic stimuli. *Pde5a*$^{-/-}$ mice are viable, fertile, have a normal life span, and were born at normal Mendelian ratios. Gross morphological inspection revealed a healthy phenotype, with no overt abnormalities and an apparently normal behavior, suggesting that loss of *Pde5a* does not affect mouse development and viability (Figure 1A and Figure S1C–F). We measured cGMP-phosphodiesterase activity in the absence and presence of the selective PDE5A inhibitor sildenafil in mouse embryonic fibroblasts (MEF) cultures derived from *Pde5a*$^{-/-}$ and wild-type (WT) mice. The analysis revealed that both the *Pde5a* ablation and pharmacological inhibition resulted in a comparable reduction of cGMP-phosphodiesterase activity (Figure S1G). Moreover, the addition of sildenafil to *Pde5a*$^{-/-}$ MEFs did not further reduce cGMP hydrolysis, confirming that sildenafil's primary target in adipocytes is the PDE5A. To test whether *Pde5*a ablation increases cGMP levels and activates the PKG signaling pathway, we analyzed the phosphorylation status of vasodilator-stimulated phosphoprotein (VASP) in the same cell extracts. We found that global *Pde5a* deficiency significantly increased PKG-dependent phosphorylation of VASP on Serine^{239} indicating heightened PKG activity (Figure S1H and I).

While histomorphometric analyses of adipose tissue depots showed no major differences in BW or fat mass under basal condition between *Pde5a*$^{-/-}$ and WT mice (Figure 1B and C), a significant reduction of adipocyte area was observed in both white and brown adipocytes of *Pde5a*$^{-/-}$ mice (Figure 1D and G). This reduction in adipocyte size is a hallmark of 'WAT-browning', a process associated with increased non-shivering thermogenesis and metabolic activity [23]. *Ucp1* is a key player in the process by which BAT increases energy expenditure [24]. To investigate whether WAT browning occurs in *Pde5a*$^{-/-}$mice,

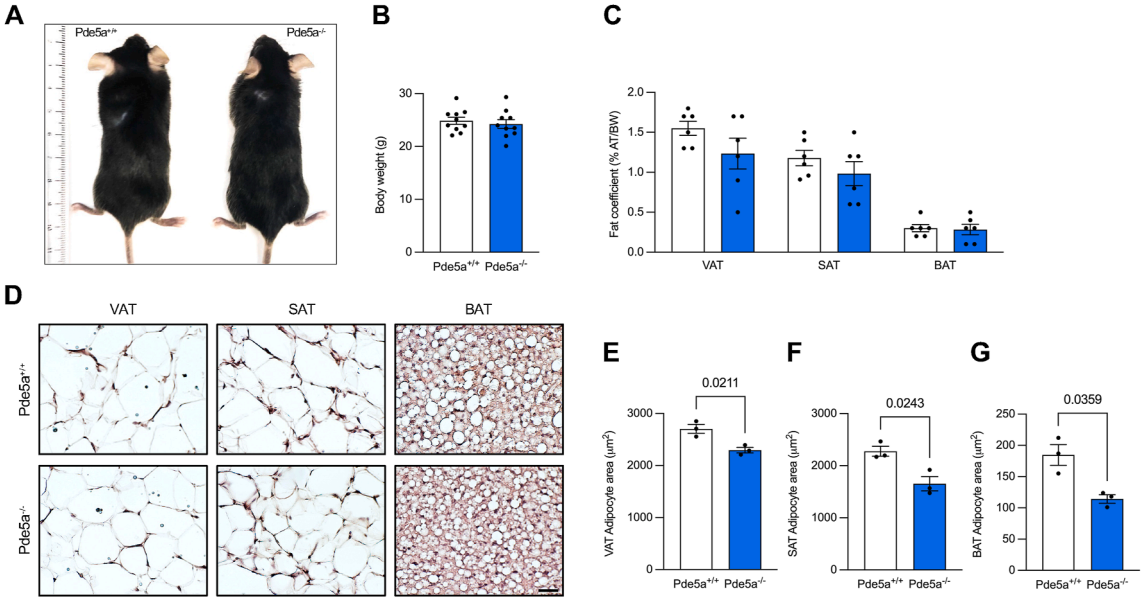

Figure 1: White adipose tissue from *Pde5a*$^{-/-}$ mice displays morphological features of brown fat. (A) Representative view of 2-month-old *Pde5a*$^{+/+}$ and *Pde5a*$^{-/-}$ male mice. **(B)** Body weight (BW) of *Pde5a*$^{+/+}$ (*n = 10*) and *Pde5a*$^{-/-}$ (*n = 10*) mice fed a normal diet. **(C)** Adipose tissue (epididymal visceral adipose tissue VAT, inguinal subcutaneous adipose tissue SAT, interscapular brown adipose tissue BAT) weight as percentage of total BW of 2-month-old *Pde5a*$^{+/+}$ (*n = 6, white*) and *Pde5a*$^{-/-}$ (*n = 6, blue*) male mice. **(D)** Hematoxylin and eosin (H&E) staining of adipose tissue sections of VAT, SAT and BAT from 2-month-old *Pde5a*$^{+/+}$ and *Pde5a*$^{-/-}$ male mice; scale bar = 50 µm. **(E–G)** Average area of adipocytes (100 cells/mouse) in FFPE sections obtained from VAT **(E)**, SAT **(F)** and BAT **(G)** of 2-month-old *Pde5a*$^{+/+}$ (*n = 3, white*) and *Pde5a*$^{-/-}$ (*n = 3, blue*) male mice. Results in scatter dot plot graphs are shown as mean ± SEM. Statistical analysis was performed using Student t-test.

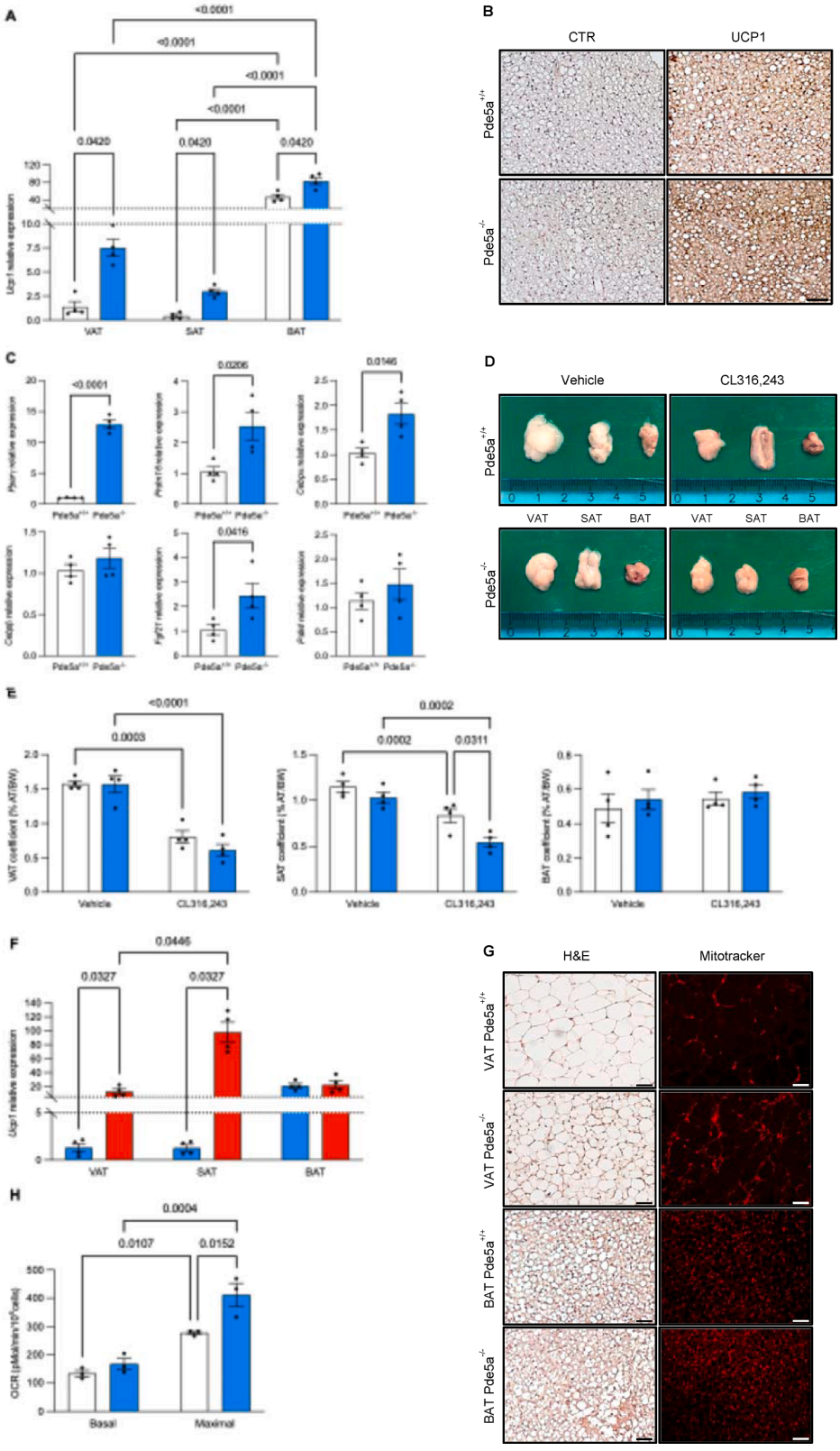

Figure 2: *Pde5a* ablation induces WAT browning and enhances thermogenic capacity. (A) qPCR gene expression analysis of *Ucp1* performed on AT depots obtained from *Pde5a*$^{+/+}$ ($n = 4$, *white*) and *Pde5a*$^{-/-}$ ($n = 4$, *blue*) mice. *Hprt1* was used as housekeeping gene for normalization. Data are presented as dot plots with column bars ± SEM showing all the experimental samples. Statistical analysis was performed using two-way ANOVA test. **(B)** Immunohistochemistry (IHC) staining of BAT sections of *Pde5a*$^{+/+}$ and *Pde5a*$^{-/-}$ mice showing increased UCP1 expression in *Pde5a*$^{-/-}$ mice as compared to WT mice. Left panels = unstained sections; right panels = UCP1 stained sections. Scale bar = 100 μm. **(C)** qPCR gene expression analysis of thermogenic markers and BAT-enriched genes performed on VAT obtained from *Pde5a*$^{+/+}$ ($n = 4$, *white*) and *Pde5a*$^{-/-}$

we analyzed the expression of canonical BAT markers. Notably, *Ucp1* expression was significantly upregulated in all adipose tissue depots of *Pde5a*$^{-/-}$ mice, suggesting that the absence of *Pde5a* promotes the "beigeing" of WAT while also fostering the thermogenic program in BAT (Figure 2A and B). In support of this observation, we found an overall increase in the expression of other thermogenic or BAT-enriched genes, including Peroxisome proliferator-activated receptor gamma (*Pparg*), PR domain containing 16 (*Prdm16*), CCAAT Enhancer Binding Protein Alpha (*Cebpα*) and Beta (*Cebpβ*), Fibroblast growth factor 21 (*Fgf21*) and Pyruvate dehydrogenase kinase isoenzyme 4 (*Pdk4*) in *Pde5a*$^{-/-}$ WAT, suggesting that *Pde5a* ablation is accompanied by an increase in '*beige*' adipocytes within WAT (Figure 2C).

To further assess the impact of *Pde5a* deletion on fat thermogenic capacity *in vivo*, *Pde5a*$^{-/-}$ mice were treated with a β3-adrenergic receptor (β3-AR) selective agonist (CL316,243) for 10 days. Macroscopic analysis of tissues from vehicle and CL316,243-treated mice revealed that fat depots from *Pde5a*$^{-/-}$ mice appeared constitutively browner in color compared to WT mice, resembling a thermogenic activated phenotype (Figure 2D). Following β3-AR agonist treatment, we found a significant reduction in visceral adipose tissue (VAT) in both *Pde5a*$^{-/-}$ and WT mice. However, this effect was not observed in the subcutaneous adipose tissue (SAT), the depot most prone to browning. In SAT, the absence of *Pde5a* resulted in a greater reduction in fat mass following adrenergic stimulation compared to WT mice (Figure 2E). This effect was accompanied by a robust increase in *Ucp1* expression in SAT from CL316,243-treated *Pde5a*$^{-/-}$ mice (Figure 2F), suggesting a pivotal role of PDE5A in regulating SAT plasticity.

Mitochondrial dynamics play a critical role in energy metabolism and glucose homeostasis [25]. To further elucidate the mechanism underlying the increased thermogenic potential in *Pde5a* KO mice, we examined mitochondria density and function in AT. This analysis revealed marked differences in adipose tissue morphology and mitochondrial content between *Pde5a*$^{-/-}$ and wild-type mice. H&E staining of VAT from *Pde5a*$^{-/-}$ mice showed reduced adipocyte size and increased cellular density compared to wild-type controls, suggestive of adipocyte remodeling and the emergence of beige-like features. In BAT, *Pde5a* deficiency was associated with denser multilocular morphology and decreased lipid droplet size, consistent with enhanced brown fat activation. These morphological changes were paralleled by Mitotracker staining, which demonstrated increased mitochondrial content in both VAT and BAT of *Pde5a* deficient mice compared to wild-type controls. Collectively, these findings indicate that *Pde5a* deletion promotes mitochondrial biogenesis and thermogenic remodeling in both brown and white adipose tissue depots, reinforcing the role of PDE5A in the regulation of adipose tissue plasticity (Figure 2G).

To assess whether the increased number of mitochondria was associated with altered mitochondrial function, we analyzed mitochondrial respiration in primary adipocytes. Basal oxygen consumption rate (OCR), a measure of mitochondrial aerobic respiration, and extracellular acidification rate (ECAR), an indicator of lactate production [26], showed a trend toward higher values in adipocytes derived from *Pde5a*$^{-/-}$ mice compared to WT controls (Figure 2H and S1J). A significant difference in OCR was observed following the addition of the uncoupler FCCP, which enables the estimation of maximal oxidative capacity. These results indicate that *Pde5a* deficiency enhances the maximal oxidative capacity of adipocytes. Importantly, this increase does not necessarily reflect enhanced thermogenesis but rather supports the notion that PDE5A influences adipose tissue plasticity by promoting the recruitment of *beige* adipocytes within WAT.

The increase in *beige* adipocytes drives the enhanced thermogenic activity, indicating that the primary role of PDE5A relies in regulating adipose tissue plasticity, rather than directly mitochondrial biogenesis. This observation is further supported by the analysis of Peroxisome proliferator-activated receptor-gamma coactivator 1 alpha (Pgc1α), whose mRNA expression levels are not significantly different in VAT from *Pde5a* KO mice compared to WT (Figure S1K).

The increased thermogenic capacity prompted us to investigate surface body temperature using infrared thermography that accurately reflects changes in BAT activity *in vivo* [27]. We measured surface body temperature of mice at room temperature (22—24 °C) and following cold exposure (4 °C). Infrared thermocamera images and surface skin temperature analysis showed that *Pde5a* KO mice display a significantly higher interscapular skin temperature, as well as greater difference between interscapular and lumbar back skin temperature compared to WT mice (Figure 3A, B—E). The same trend can be observed during cold exposure, with statistical significance emerging after normalization for the lumbar surface temperature, as expected. This is consistent with the observation that interscapular BAT in the WT appropriately responds to cold challenge, while BAT in the *Pde5a* deficient mice is already basally more activated, even at room temperature (Figure 3C—E). In summary, these data demonstrate that constitutive *Pde5a* ablation induces WAT browning and enhances thermogenic capacity *in vivo*, suggesting that PDE5A plays a pivotal role in modulating the thermogenic program.

3.2. Pde5a deficiency prevents aging-related liver steatosis and diet-induced obesity

To determine the long-term effect of having an enhanced browning *in vivo*, we performed abdominal magnetic resonance imaging (MRI) in 12-month-old mice. Imaging analysis clearly showed that *Pde5a*$^{-/-}$ mice display reduced visceral and subcutaneous fat volumes compared to controls (Figure 3F and G). Notably, a striking difference in liver fat fraction (FF) and apparent diffusion coefficient (ADC) was observed, with *Pde5a* deficient mice showing markedly lower levels (Figure 3H—J). Subsequent histological analysis of liver sections confirmed protection against aging-induced liver steatosis, as demonstrated by the absence of hepatocyte ballooning and inflammatory infiltrates in the liver parenchyma (Figure 3K). Having established that *Pde5a* deficiency may confer protection against age-

(*n = 4, blue*) mice. *Hprt1* was used as housekeeping gene for normalization. Data are presented as dot plots with column bars ± SEM. Statistical analysis was performed using Student t-test. **(D)** Representative fat pads images of *Pde5a*$^{+/+}$ and *Pde5a*$^{-/-}$ mice following saline (vehicle) or CL316,243 injection. **(E)** Adipose tissue depots weight as a percentage of total BW of *Pde5a*$^{+/+}$ (*n = 4, white*) and *Pde5a*$^{-/-}$ (*n = 4, blue*) mice following saline or CL316,243 treatment. Data are presented as dot plots with column bars ± SEM. Statistical analysis was performed using two-way ANOVA test. **(F)** qPCR gene expression analysis of *Ucp1* performed on adipose tissue depots obtained from *Pde5a*$^{-/-}$ mice following saline (*n = 4, blue*) and CL316,243 (*n = 4, red*) treatment. *Hprt1* was used as housekeeping gene for normalization. Data are presented as dot plots with column bars ± SEM. Statistical analysis was performed using two-way ANOVA test. **(G)** H&E staining and Mitotracker staining from WT and *Pde5a*$^{-/-}$ VAT and BAT. Scale bar = 50 μm. **(H)** Respiration and glycolysis analysis on VAT cultures from *Pde5a*$^{+/+}$ (*n = 3, white*) and *Pde5a*$^{-/-}$ (*n = 3, blue*) mice through quantification of basal and maximal oxidative capacity trough oxygen consumption rate (OCR). Data are presented as dot plots with column bars ± SEM. Statistical analysis was performed using Student t-test.

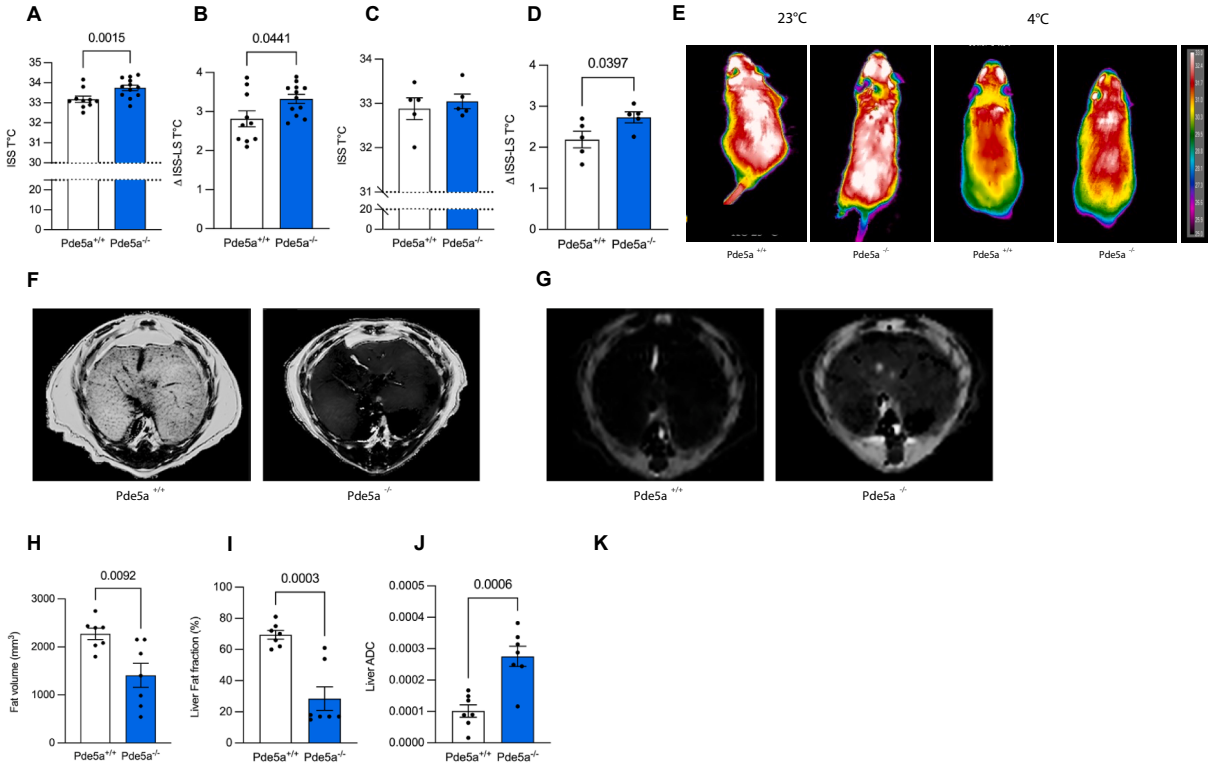

Figure 3: ***Pde5a*** **deficiency increases energy expenditure and thermogenic capacity in vivo. (A—D)** Quantification of average interscapular surface skin temperature (ISS) and delta interscapular skin surface temperature and lumbar surface temperature (ISS-LS) on $n = 10$ *Pde5a*$^{+/+}$ mice and $n = 12$ *Pde5a*$^{-/-}$ mice/each group at 23 °C **(A—B)** and 4 °C **(C—D)**. Data are presented as dot plots with column bars ± SEM. Statistical analysis was performed applying one-way ANOVA test for upper panels and ANCOVA test comparing post-exposure temperature values and accounting for baseline temperature values as covariate. **(E)** Representative infrared imaging of *Pde5a*$^{+/+}$ and *Pde5a*$^{-/-}$ mice under room temperature (23 °C) or after cold exposure (4 °C). **(F—G)** Exemplificative liver Fat Fraction **(F)** and Apparent Diffusion Coefficient **(G)** MRI maps of *Pde5a*$^{+/+}$ and *Pde5a*$^{-/-}$. **(H—J)** Dot plot analysis of subcutaneous and visceral fat volume **(H)**, liver fat fraction **(I)** and liver apparent diffusion coefficient **(J)**. Results in scatter dot plot graphs are shown as mean ± SEM (n = 7 for each group). Statistical analysis was performed using Student t-test. **(K)** H&E staining of liver sections from 12-month-old *Pde5a*$^{+/+}$ and *Pde5a*$^{-/-}$ male mice; scale bar = 50 μm.

related metabolic alterations, we next investigated whether also protects against diet-induced metabolic challenges.

First, *Pde5a* KO mice were subjected to either a normal chow (NC) or high-fat diet (HFD) for 12 weeks, following the experimental protocol outlined in Figure S1L. Mice fed with NC showed no significant changes in BW; however, when on an HFD, body mass dramatically increased in WT but much less in *Pde5a* KO mice, starting from the fourth week of dietary challenge (Figure 4A and B).

Second, HFD is typically associated with dyslipidemia, peripheral insulin resistance and glucose intolerance [28]. Remarkably, *Pde5a* deficient mice were resistant to the hyperglycemia and hyperinsulinemia induced by the HFD (Figure 4C and D). Consistent with these findings, HFD-fed *Pde5a*$^{-/-}$ mice displayed a significant reduction of fat mass compared to HFD-fed WT mice, which aligned with the differences observed in main adipose tissue depots (Figure 4E—G). Notably, these differences were not attributable to statistically significant variations in food intake. However, we acknowledge that even a minor, non-significant reduction in caloric intake in *Pde5a*$^{-/-}$ mice could contribute, at least partially, to the observed phenotype (Figure S1M). Additionally, no significant difference in physical activity, measured by total distance traveled, were observed between the two groups (Figure S1N). Conversely, the food efficiency ratio (FER), calculated as the ratio of weight gain to food intake, which was similar in both genotypes under NC, was significantly lower in *Pde5a* deficient mice under HFD (Figure 4H).

Third, HFD feeding is known to cause liver damage due to lipid accumulation and systemic chronic low-grade inflammation [29,30]. In agreement with the observed metabolic findings, HFD-fed *Pde5a*$^{-/-}$ mice were protected from HFD-induced liver steatosis (Figure 4I and J) and exhibited lower serum levels of pro-inflammatory cytokines IL1α and IFNγ (Figure S1O and P). Together, these findings demonstrate that constitutive deletion of *Pde5a* protects mice from both aging and diet-induced obesity, while mitigating hepatic steatosis and inflammation.

3.3. Pde5a ablation affects glucose homeostasis and adipokines' profile

To further investigate the metabolic phenotype associated to *Pde5a* deficiency, we assessed whole-body glucose homeostasis by measuring plasma glucose levels and insulin sensitivity in normal chow-fed mice. Both the Glucose Tolerance Test (GTT) and Insulin Tolerance Test (ITT) showed that, while fasting glucose levels were similar between the two genotypes, the early glucose response (15—30 min) following glucose administration was unexpectedly higher in *Pde5a*$^{-/-}$ than WT mice, before returning to similar levels at 60 min and thereafter (Figure 5A and B). Interestingly, insulin levels were nearly identical at all time points. Since the initial response to glucose

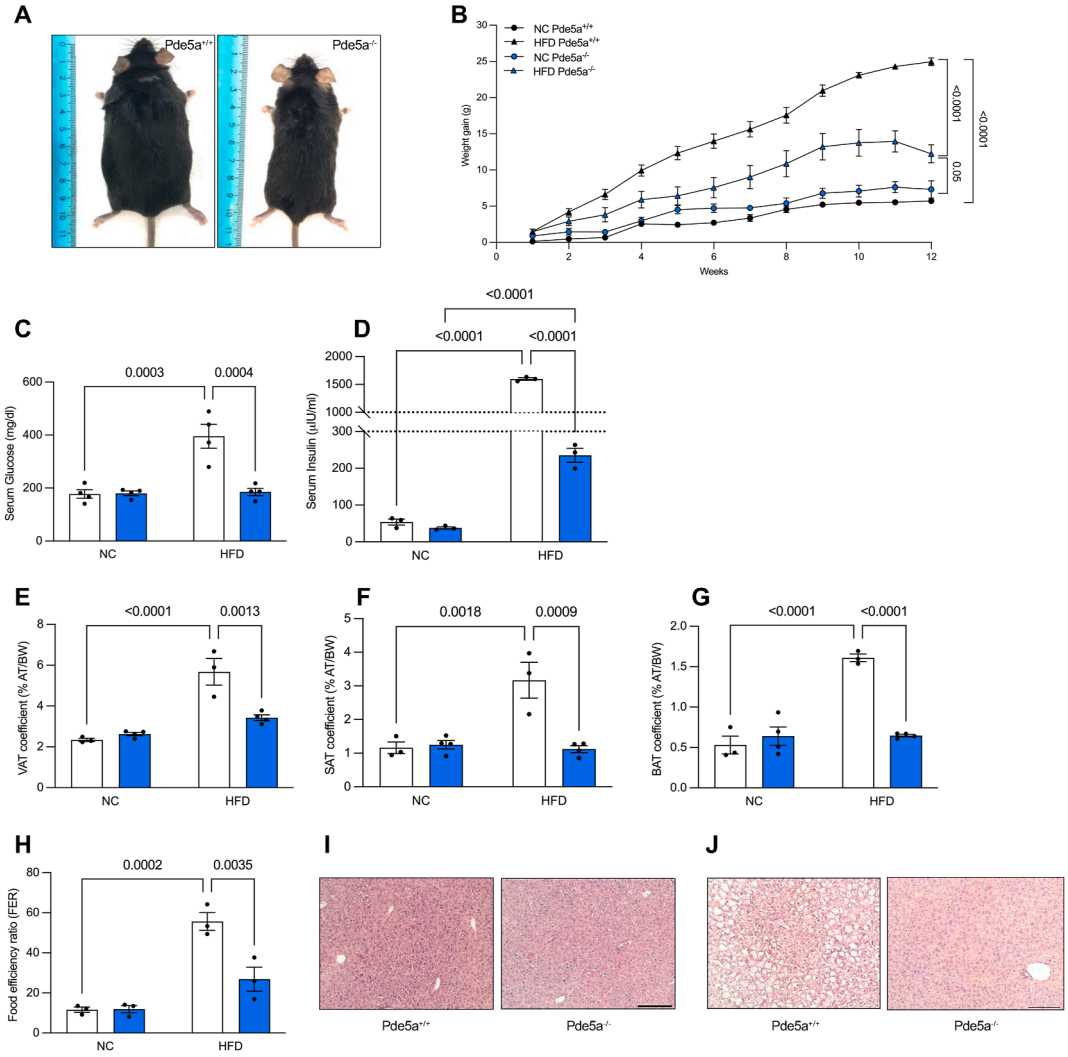

Figure 4: *Pde5a* deletion confers protection from DIO. (A) Dorsal view of *Pde5a*$^{+/+}$ and *Pde5a*$^{-/-}$ male mice after 12 weeks feeding with HFD at age of 6-month-old**. (B)** Relative change in BW (weight gain) of *Pde5a*$^{-/-}$ and their control littermates fed with HFD or NC over 12 weeks, showing onset of obesity in WT but not in Pde5$^{-/-}$ mice (n = 9 each group). Data are expressed as mean ± SEM. Statistical analysis was performed applying a three-way ANOVA test. **(C–D)** Measurements of fasting serum glucose **(C)** and insulin **(D)** levels in *Pde5a*$^{-/-}$ (*blue*) and WT (*white*) mice after 12 weeks feeding with NC and HFD (n = 4). Data are presented as dot plots with column bars ± SEM. Statistical analysis was performed using two-way ANOVA test. **(E–G)** Adipose tissue depots weight as a percentage of total BW of *Pde5a*$^{+/+}$ (*white*) and *Pde5a*$^{-/-}$ (*blue*) mice after 12 weeks feeding with NC and HFD (n = 4 each group). Data are presented as dot plots with column bars ± SEM. Statistical analysis was performed using two-way ANOVA test. **(H)** Food efficiency ratio (FER) as percentage of weight gain/food intake in *Pde5a*$^{-/-}$ (*blue*) and WT (*white*) mice after 12 weeks feeding with NC (n = 10) and HFD (n = 10). Data are presented as dot plots with column bars ± SEM. Statistical analysis was performed using two-way ANOVA test. **(I–J)** H&E staining of liver from *Pde5a*$^{+/+}$ and *Pde5a*$^{-/-}$ mice after 12 weeks feeding with NC **(I)** and HFD **(J)**. Scale bar = 100 µm.

infusion is typically associated with a stop of hepatic glucose outflow, the observation that the fasting, 60 and 120 min glucose levels, as well as insulin at all time points, were identical between groups, suggest that *Pde5a*$^{-/-}$ mice exhibit a normal insulin sensitivity, but altered hepatic glucose output (Figure 5A and B and Figure 4C and D). Thus, the transient difference in early response to glucose infusion seems mainly due to a more efficient reduction in liver glucose output in the WT.

To complete the metabolic characterization of these mice, we also measured adipokines, which interact dynamically with insulin to ensure metabolic homeostasis [31]. Under physiological conditions, serum levels of adiponectin and leptin are inversely correlated, with obesity typically associated with elevated leptin and decreased adiponectin levels [32]. *Pde5a*$^{-/-}$ mice displayed significantly lower levels of leptin and higher levels of adiponectin (Figure 5C and D), resulting in a marked reduction in the adiponectin/leptin ratio (Figure 5E), a surrogate marker of metabolic impairment. These findings are supported by the corresponding changes in the expression of *Lep* and *Adipoq* genes in WAT (Figure 5F and G). The mitigated weight gain in *Pde5a* KO mice under HFD was accompanied by significantly lower serum insulin and glucose levels, alongside higher levels of adiponectin (Figure 4C and D). Surprisingly, however, there was no difference in plasma leptin levels under HFD (Figure 5C), suggesting a dissociation among adipocyte size area, fat depots

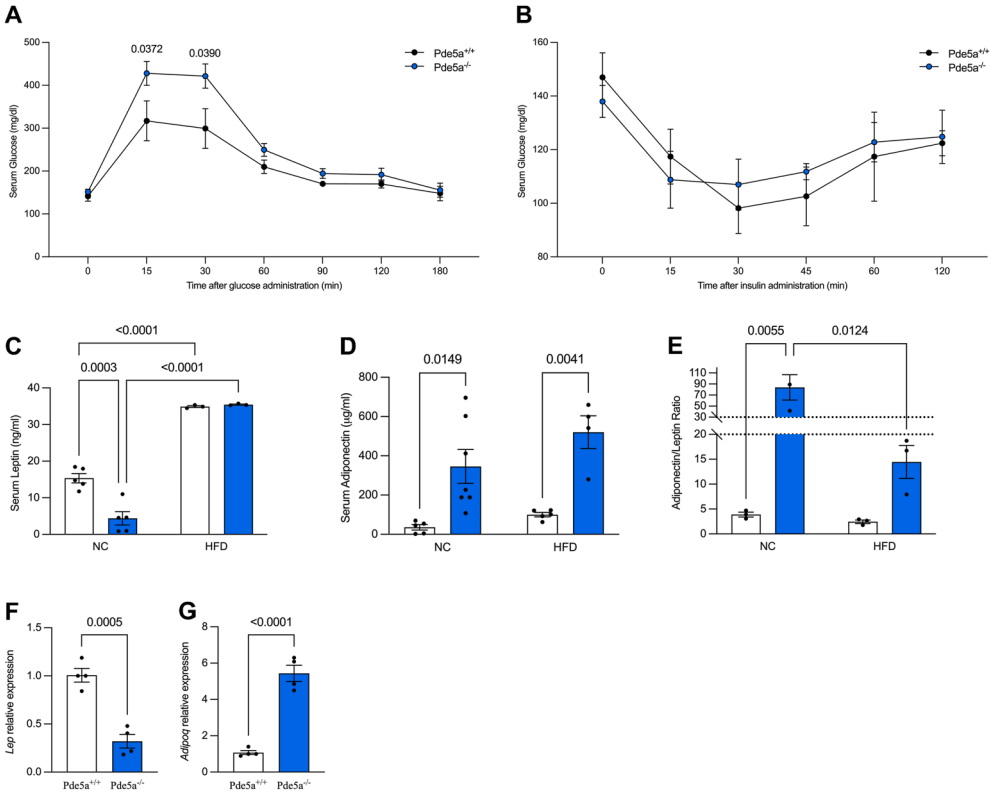

Figure 5: *Pde5a* deficiency confers a constitutive metabolic healthy phenotype to mice. (A–B) i.p. glucose tolerance test (IPGTT, **A**) and i.p. insulin tolerance test (IP-ITT, **B**) in 2-month-old *Pde5a*$^{+/+}$ (*white*) and *Pde5a*$^{-/-}$ (*blue*) male mice (n = 5/group). Average body weight is 26,5g ± 0,2 for WT and 26,1g ± 0,3 for *Pde5a*$^{-/-}$ mice. Statistical analysis was performed using Student t-test. **(C)** Measurements of serum leptin levels in *Pde5a*$^{-/-}$ (*blue*) and WT (*white*) mice after 12 weeks feeding with NC (n = 5) and HFD (n = 3). Data are presented as dot plots with column bars ± SEM. Statistical analysis was performed using two-way ANOVA test. **(D)** Measurements of serum adiponectin levels in *Pde5a*$^{-/-}$ (*blue*) and WT (*white*) mice after 12 weeks feeding with NC (n = 5) and HFD (n = 4). Data are presented as dot plots with column bars ± SEM. Statistical analysis was performed using two-way ANOVA test. **(E)** Measurement of Adiponectin/Leptin ratio in *Pde5a*$^{-/-}$ (*blue*) and WT (*white*) mice after 12 weeks feeding with NC (n = 5) and HFD (n = 4). Data are presented as dot plots with column bars ± SEM. Statistical analysis was performed using two-way ANOVA test. **(F–G)** qPCR gene expression analysis of *Lep* **(F)** and *AdipoQ* **(G)** performed on visceral adipose tissue obtained from *Pde5a*$^{+/+}$ (*n = 4, white*) and *Pde5a*$^{-/-}$ (*n = 4, blue*) mice. *Hprt1* was used as housekeeping gene for normalization. Data are presented as dot plots with column bars ± SEM. Statistical analysis was performed using Student t-test.

mass, and adipokine expression. Collectively, these data support a shift in adipose tissue plasticity triggered by *Pde5a* deficiency.

3.4. Pde5a deletion triggers organ-specific reprogramming of glucose usage and fatty acids metabolism

We employed Nuclear Magnetic Resonance (NMR)-based metabolomic to analyze glucose-responsive tissues from starved mice and after glucose administration (metabolic challenge). Fasting data did not reveal striking differences between the two genotypes (data not shown), consistently with the grossly normal phenotype of *Pde5a*$^{-/-}$ under basal conditions. Distinct metabolic responses were, however, evident under metabolic challenge. Resonance assignment for each matrix for both for ^{1}H and ^{13}C nuclei are provided in Table S1. The use of [1,2,3,4,5,6-$^{13}C_6$] glucose in conjunction with 1^{13}C-NMR spectroscopy enabled the labeling of intermediates to investigate the metabolic pathways involved in glucose utilization. ^{13}C labeling was applied to liver, kidney, VAT, BAT and serum. However, labeled isotopomers were detected exclusively in the liver and kidney, likely due to the lower concentration of labeled metabolites in other tissues, which hindered a robust resonance detection (data not shown). The ^{1}H-NMR liver spectra after glucose administration produced a Partial Least Squares Discriminant Analysis (PLS-DA) model with strong prediction accuracy (91 %) and precision (94 %). Notably, bile salts and glucose-1-phosphate levels were significantly higher in *Pde5a*$^{-/-}$ mice, while levels of long-chain fatty acids, triacylglycerols, organic acids, lactate, choline, aa, and glucose were lower. Regression coefficient analysis also revealed that Pde*5a* deficiency leads to lower levels of 3-hydroxybutyrate, a ketone body generated by β-hydroxybutyrate dehydrogenase activity in the ketogenetic pathway (Figure 6A). The ^{13}C-NMR liver spectra displayed complex patterns, documenting the presence of various isotopologue species (Table S1). From ^{13}C-NMR liver spectra, 11 different labeled metabolites were identified. Metabolites derived from glycolysis revealed that *Pde5a*$^{-/-}$ mice exhibited significantly lower levels of lactate and glycerol moiety of triglyceride isotopomers compared to WT mice (Tables S2 and 3 and Figure S2A). Notably, we did not observe the presence of labeled glutamate [4,5-$^{13}C_2$] in either *Pde5a*$^{+/+}$ and *Pde5a*$^{-/-}$ mice, suggesting that the Acetyl-CoA involved in the TCA cycle is primarily derived from β-oxidation of fatty acids rather than glycolysis. In addition, the glucose isotopomers ratios indicate that gluconeogenesis did not vary between genotypes, as evidenced by similar production of [2,3,4,5,6-$^{13}C_5$] glucose. Overall, liver metabolomics data showed a reduction in lactate and alanine concentrations, supporting a shift in glucose flux towards glycogen synthesis, rather than

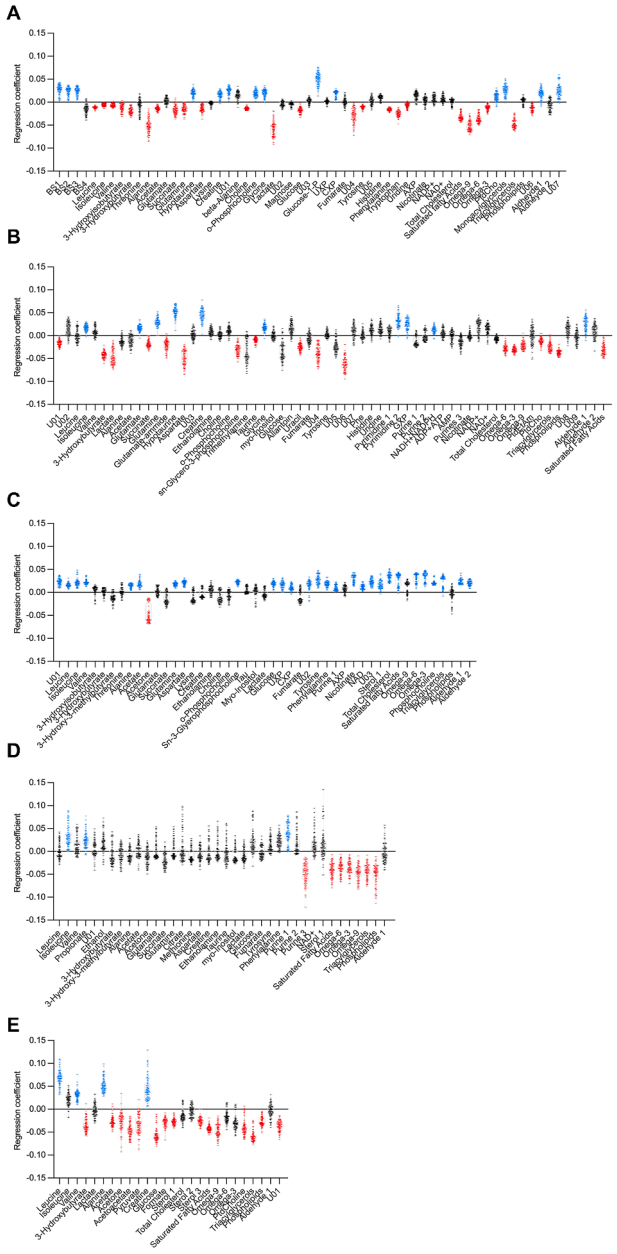

Figure 6: NMR reveals metabolic pathways constitutively altered in *Pde5a* deficient mice. Panel for the PLS-DA model of insulin sensitive tissues and serum obtained from Pde5 KO and WT mice after glucose administration. Regression coefficient values are shown for liver **(A)**, kidney **(B)**, BAT **(C)**, VAT **(D)** and serum **(E)**. Variables significantly higher in *Pde5a* KO are depicted in *blue*, variables significantly lower in *Pde5a* deficient mice are depicted in *red* and non-significantly modulated variables are shown in *black*.

glycolysis. This fits with the higher glucose-1-phosphate observed in ^{1}H-NMR experiment, and lower ^{13}C labelling in glycolysis intermediates, as well as a reduced glycerol moiety labeling in triglycerides. The preferential storage of glucose into glycogen of *Pde5a*$^{-/-}$ mice, also explains their lower glucose liver output that accounts for the differential early serum response during glucose infusion test.

In the kidney, ^{1}H-NMR spectra highlighted 62 metabolites (Table S1). The PLS-DA model showed 82 % accuracy and 78 % precision, with significant higher levels of glutamine, hypo taurine, creatine, pyrimidine compound, and GTP in *Pde5a*$^{-/-}$ mice (Figure 6B). Conversely, aspartate, 3-hydroxybutyrate, lactate, lipids and phospholipids were lower in *Pde5a*$^{-/-}$ mice after metabolic challenge. ^{13}C-NMR data from kidney samples revealed 14 labeled intermediates. The presence of labeled glutamate [4,5-$^{13}C_2$] indicates the incorporation of labeled Acetyl-CoA derived from the glycolytic pathway, in contrast to what is observed in the liver. Yet, the observation that glutamate [4,5-$^{13}C_2$] production is still reduced in the kidney of *Pde5a*$^{-/-}$ mice, confirms data obtained in the liver pointing out toward a globally reduced glucose [1,2,3,4,5,6-$^{13}C_6$] flux through the glycolytic pathway (Figure S2B and Tables S1–3), and the use of amino acids as alternative energy source.

Adipose tissue NMR analysis complemented the findings observed in the liver and kidney. The PLS-DA model for BAT following glucose administration demonstrated a clear separation between WT and *Pde5a*$^{-/-}$ mice (92 % accuracy and 88 % precision). Most significant metabolites, including aa, organic acids, bile salts (BS1), glycerophosphocholine, phosphocholine, glucose, NAD, and lipids were positively correlated with the *Pde5a*$^{-/-}$ genotype, except for acetone, which was negatively correlated (Figure 6C). Similarly, the PLS-DA model for VAT indicated reduced levels of long-chain fatty acids and phospholipids in *Pde5a*$^{-/-}$ mice (Figure 6D).

Finally, serum NMR data after glucose administration recapitulates the metabolic shift observed in the other tissues, with a clear genotype separation (85 % accuracy and 85 % precision) and a significant negative variation for lipids and ketone bodies, as inspected by PLS-DA model (Figure 6E).

Overall, the combined labeled (^{13}C and ^{1}H) and unlabeled NMR analyses suggest that *Pde5a* deficiency triggers significant metabolic reprogramming, affecting various tissues. This is particularly evident following metabolic challenges, especially in the liver, kidney, and BAT. These changes hint at an adaptive shift in glucose and lipid handling derived from *Pde5a*'s regulation of tissue-specific metabolism.

3.5. Pde5a KO mice display increased cAMP-PKA signaling in adipose tissue

The peculiar metabolic activation observed in BAT prompted us to explore the underlying molecular mechanism. The cAMP-PKA signaling pathway is considered crucial for browning phenotype and thermogenic activation [33]. In adipocytes, cAMP levels are regulated by cGMP-inhibited phosphodiesterase 3 (PDE3), with the *Pde3b* isoform being highly expressed in adipose tissues [34]. Previous studies have shown that *Pde3b* ablation confers resistance against HFD, by promoting WAT browning due to the activation of AMPK signaling [35,36]. Starting from these premises, we hypothesized that an interaction between cGMP and cAMP pathways might occur in *beige* adipocytes of *Pde5a*$^{-/-}$ mice. Surprisingly, we found a significantly reduction of *Pde3b* mRNA levels in *Pde5a* KO WAT (Figure 7A), leading to elevated cAMP levels (Figure 7B). The increase in cAMP was able to activate PKA, as evidenced by enhanced phosphorylation of PKA-substrates (Figure 7C), without compensatory change in the expression of other PDEs (Figure S3A).

To further explore the PDE5A-PDE3B crosstalk, we performed in vitro silencing experiments in 3T3-L1 adipocytes. Silencing of *Pde3b* decreased *Pde5a* mRNA levels (Figure 7D and E), suggesting that *Pde3b* positively regulates *Pde5a* transcription. The

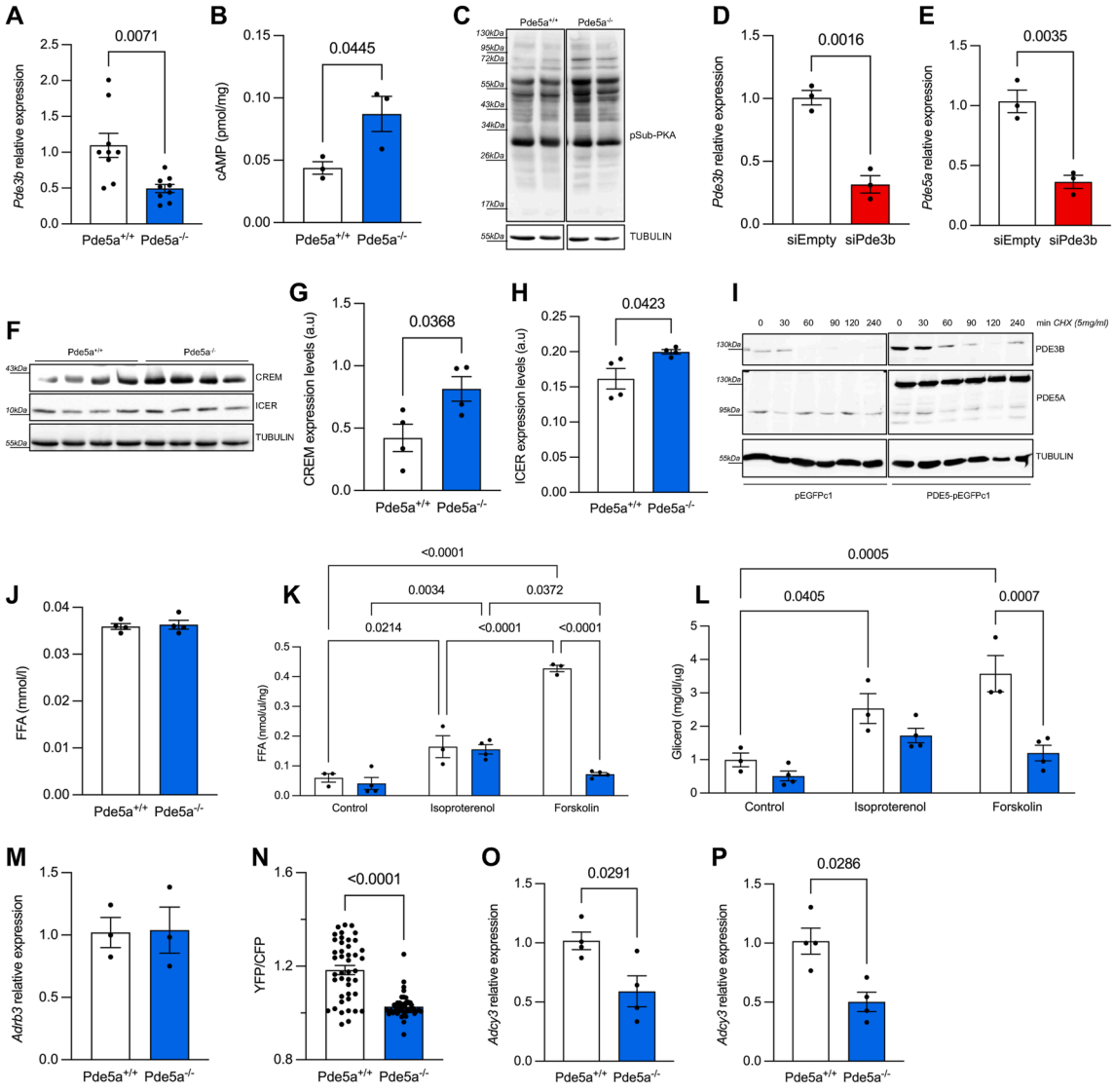

Figure 7: *Pde5a* KO mice display increased cAMP-PKA signaling and impaired Adenylate Cyclase activity. (A) qPCR gene expression analysis of *Pde3b* performed on VAT obtained from *Pde5a*$^{+/+}$ ($n = 9$, *white*) and *Pde5a*$^{-/-}$ ($n = 9$, *blue*) mice. *Hprt1* was used as housekeeping gene for normalization. Data are presented as dot plots with column bars ± SEM. Statistical analysis was performed using Student t-test. **(B)** Quantification of intracellular cAMP levels in VAT lysates obtained from *Pde5a*$^{+/+}$ ($n = 3$, *white*) and *Pde5a*$^{-/-}$ ($n = 3$, *blue*) mice. Data are presented as dot plots with column bars ± SEM. Statistical analysis was performed using Student t-test. **(C)** Representative immunoblots of phosphorylated PKA substrates protein levels in whole lysates obtained from VAT of *Pde5a*$^{+/+}$ and *Pde5a*$^{-/-}$ mice. TUBULIN was used as housekeeping gene for normalization. **(D–E)** qPCR gene expression analysis of *Pde5a* **(D)** and *Pde3b* **(E)** performed on 3T3-L1 cells transiently silenced with *siPde3b* or scramble control (siEmpty). **(F)** Immunoblots of CREM and ICER protein levels in whole lysates obtained from VAT of *Pde5a*$^{+/+}$ and *Pde5a*$^{-/-}$ ($n = 4$) mice. TUBULIN was used as housekeeping gene for normalization. **(G–H)** Densitometric analyses for CREM **(G)** and ICER **(H)** immunoblots. Data are presented as dot plots with column bars ± SEM. Statistical analysis was performed using Student t-test. **(I)** Representative immunoblot showing PDE3B and PDE5A expression in 3T3-L1 cells transfected with GFP-PDE5A plasmid or empty GFP plasmid, treated with or without 5 mg/mL cycloheximide (CHX) for the indicated time (0-4h). TUBULIN was used as housekeeping gene for normalization. **(J–L)** Basal and stimulated lipolysis evaluation through serum free fatty acids quantification in *Pde5a*$^{+/+}$ and *Pde5a*$^{-/-}$ ($n = 3$) mice **(J)**. Free fatty acids (FFA, **K**) and glycerol (**L**) quantification in adipocytes isolated from *Pde5a*$^{+/+}$ and *Pde5a*$^{-/-}$ ($n = 4$) VAT after lipolysis stimulation with 10 μM forskolin/isoproterenol. Data are presented as dot plots with column bars ± SEM. Statistical analysis was performed using Student t-test (J) or two-way ANOVA test (K–L). **(M)** qPCR gene expression analysis of *Adrb3* performed on VAT obtained from *Pde5a*$^{+/+}$ ($n = 3$, *white*) and *Pde5a*$^{-/-}$ ($n = 3$, *blue*) mice. *Hprt1* was used as housekeeping gene for normalization. Data are presented as dot plots with column bars ± SEM. **(N)** Normalized YFP/CFP FRET ratio on MEFs isolated from *Pde5a*$^{+/+}$ and *Pde5a*$^{-/-}$ mice transfected for 48h with AKAR3 PKA sensor and stimulated with 1 μM forskolin. Data are presented as dot plots (n = 50) with column bars ± SEM derived from three independent experiments. Statistical analysis was performed using Student t-test. **(O-P)** qPCR gene expression analysis of *Adcy3* performed on visceral adipose tissue **(O)** and MEFs **(P)** obtained from *Pde5a*$^{+/+}$ ($n = 4$, *white*) and *Pde5a*$^{-/-}$ ($n = 4$, *blue*) mice. *Hprt1* was used as housekeeping gene for normalization. Data are presented as dot plots with column bars ± SEM. Statistical analysis was performed using Student t-test.

downregulation of *Pde3b* observed in the *beige* adipose tissue AT from *Pde5a* KO mice appears to be mediated by increased levels of the transcriptional repressor CREM/ICER, which is activated in response to cAMP rise (Figure 7F–H). To test whether PDE5A stabilizes PDE3B protein, we also treated *Pde5a*-overexpressing 3T3-L1 cells with the protein synthesis inhibitor cycloheximide (CHX). As shown in Figure 7I, PDE5A over-expression not only increases PDE3B basal expression but also

delays its degradation further supporting *Pde5a* and *Pde3b* interaction in adipocytes.
Collectively these findings demonstrate that WAT to *beige* conversion of adipocytes observed in *Pde5a* KO mice results from the convergence between cAMP-PKA and cGMP-PKG signaling pathways.

3.6. Pde5a deficiency impairs Adenylate Cyclase activity

Despite the augmented cAMP-PKA signaling, we observed an overall lowering of free fatty acid (FFA) levels, glycerol moiety, and β-oxidation rate in *Pde5a* KO mice (Figure 6A—E). This led us to examine lipolysis, a key process regulated by cAMP induced phosphorylation of perilipin and hormone sensitive lipase (HSL), which catalyzes triglycerides and diglycerides breakdown, resulting in the release of FFA and glycerol [37,38]. Contrary to expectations, global deletion of *Pde5a* did not stimulate basal lipolysis (Figure 7J). Although *Pde5a* KO VAT responded similarly to WT to the β-ARs receptor activation with isoproterenol, it failed to respond to forskolin, suggesting hypo-activation of adenylate cyclase (AC), the enzyme responsible for synthesizing cAMP from ATP [1] (Figure 7K—M). Using a fluorescence resonance energy transfer (FRET)-based sensor targeting PKA activity (AKAR3) [39] we demonstrated that when overexpressed in MEFs from *Pde5a* KO mice and stimulated with isoproterenol, the PKA sensor exhibited similar FRET changes (data not shown). In contrast, MEFs stimulation with forskolin resulted in a reduced FRET ratio, confirming the hypo-responsiveness of AC to forskolin observed in *Pde5a* deficient VAT (Figure 7N).
This observation prompted us to investigate AC expression in *Pde5a* KO mice. Notably, the AC3 isoform (encoded by *Adcy3*), the most abundantly expressed in VAT and MEFs, was significantly reduced in *Pde5a* deficient tissues and primary cells (Figure 7O and P). In the $Pde5a^{-/-}$ mice, this compensatory mechanism may serve to counteract the constitutive increase of cAMP levels caused by *Pde3b* downregulation.

3.7. Adipocyte-specific Pde5a deletion is not sufficient to protect mice from diet-induced obesity

The data so far indicate a metabolic reprogramming driven by an adipose tissue crosstalk between *Pde5a*/*Pde3b* and AC-cAMP-PKA. To determine at which stage this new equilibrium is established, we crossed mice harboring *LoxP*-flanked *Pde5a* alleles ($Pde5a^{LoxP/LoxP}$) with transgenic mice expressing adiponectin promoter driven Cre recombinase ($Adipoq^{Cre}$) obtaining a mouse with committed adipocytes lacking *Pde5a* ($Pde5a^{Adpn\text{-}cKO}$) (Figure 8A and Figure S3B). The *Adipoq-Cre* recombination occurs only in mature adipocytes [40,41]. $Pde5a^{Adpn\text{-}cKO}$ mice display only a 25 % reduction of *Pde5a* mRNA levels in VAT (Figure 8B) confirming previous observation of a predominant *Pde5a* expression in adipose endothelial cells compared to mature adipocytes [4,42,43]. A parallel reduction in *Pde3b* expression was detected in the same samples (Figure 8C), however, there were no differences in BW when $Pde5a^{Adpn\text{-}cKO}$ mice were fed with HFD, suggesting that the mature adipocyte-specific loss of *Pde5a* is not sufficient to trigger metabolic reprogramming in these animals (Figure 8D). To explore this further, we crossed $Pde5a^{LoxP/LoxP}$ mice with transgenic mice expressing Cre recombinase driven by the adipocyte protein-2 (*aP2/Fabp4*) promoter ($aP2^{Cre}$), that is activated earlier in developing adipocytes ($Pde5a^{Fabp4\text{-}cKO}$) [44] (Figure 8E and Figure S3C). $Pde5a^{Fabp4\text{-}cKO}$ mice displayed a greater reduction (>40 %) in *Pde5a* expression levels in VAT than $Pde5a^{Adpn\text{-}cKO}$, and an even greater reduction (≅85 %) in *Pde3b* levels (Figure 8F—G), once again confirming the interaction between the two enzymes. Unexpectedly, no differences in BW were observed between $Fabp4^{Cre}$ positive mice and control littermates (Figure S3D), even after 12 weeks of HFD feeding (Figure 8H). This suggests that protective metabolic effect of PDE5A deletion may require complete suppression of PDE5A activity, or that an earlier developmental window is critical for these changes.

3.8. Postnatal deletion of Pde5a does not confer metabolic protection in mice

To determine the temporal window within which the metabolic healthy phenotype observed in the constitutive knockout is established, we crossed $Pde5a^{LoxP/LoxP}$ mice with $Rosa26^{CreERT}$ mice. Unlike *Pde5a* KO, which result in prenatal deletion across all tissues, $Pde5a^{CreERT\text{-}cKO}$ mice development allows for precise temporal control of *Pde5a* deletion upon tamoxifen administration. This enables to distinguish between embryonic programming effects and postnatal developmental adaptation to lifelong *Pde5a* absence.
Even in this model tamoxifen $Pde5a^{CreERT\text{-}cKO}$ produced a markedly reduction of *Pde5a* and *Pde3b* in VAT (Figure 8I—K), however these mice were not protected from HFD-induced metabolic consequences (Figure 8L), suggesting that the metabolic reprogramming must occur early during embryonic development.
We therefore isolated embryonic fibroblasts from WT and *Pde5a* KO embryos at 13.5 days post coitum (dpc). These cells serve as a reliable source of multipotent cells with multilineage potential and, under appropriate culture conditions, can effectively differentiate into adipogenic, chondrogenic, and osteogenic lineages [45]. MEFs from *Pde5a* KO mice display a lower proliferation rate compared to WT, but increased differentiation capacity into adipocytes, particularly at early stages of adipogenic differentiation (Figure S3E and F). qPCR analysis revealed upregulation of *Pparg*, a master regulator of adipogenesis, suggesting that PDE5A plays a role in the fine-tuning of adipogenesis (Figure S3G).

3.9. Gene network analysis confirms metabolic reprogramming

To better characterize the cellular and molecular mechanisms involved in metabolic reprogramming observed in *Pde5a* KO mice, we performed an in-depth analysis of the transcriptome on AT and liver from *Pde5a* deficient mice. RNA-seq of VAT and liver from *Pde5a* KO mice confirmed significant transcriptional changes. In VAT 643 genes were differentially expressed, with a strong upregulation of pathways related to thermogenesis. The Gene Ontology (GO) analysis indicated that *Pde5a* KO VAT showed significant upregulation of GO terms associated with thermogenesis, cAMP-signaling, AMPK signaling, D-aa metabolism, carbohydrate metabolism, and pyruvate metabolism, alongside downregulation of glycolysis/gluconeogenesis and lipid biosynthesis (Figure S4A—C). Notably, we found several AMPK signaling related-genes (*Map2k2, Rps6kb1, Atf4, Ngf, Hcar1* and *Arrb1*) significantly upregulated in *Pde5a* deficient VAT (Figure S4A). Compared to WT, analysis of BAT from $Pde5a^{-/-}$ mice revealed 538 differentially expressed genes, with 382 genes upregulated and 156 downregulated. GO analysis revealed an increase in genes linked to improved carbohydrate metabolism, lipid metabolism, glutathione metabolism, glycolysis/gluconeogenesis, and glycine, serine and threonine metabolism, as well as adipocytokine and insulin signaling. Conversely, gene associated to NF-kappa B signaling pathway and processes related to the degradation of valine, leucine and isoleucine were downregulated in BAT from *Pde5a* KO mice (Figure S4D—F). Like in white adipose tissue, many genes related to AMPK signaling (*Cacna1s, Hcn2, Creb3l3, Pik3r5, Cacna1d, Cd14, Adra2b, Plcb4* and *Cacna2d1*) were significantly upregulated in brown adipose tissue from $Pde5a^{-/-}$ mice (Figure S4D) suggesting a constitutive AMPK activation.

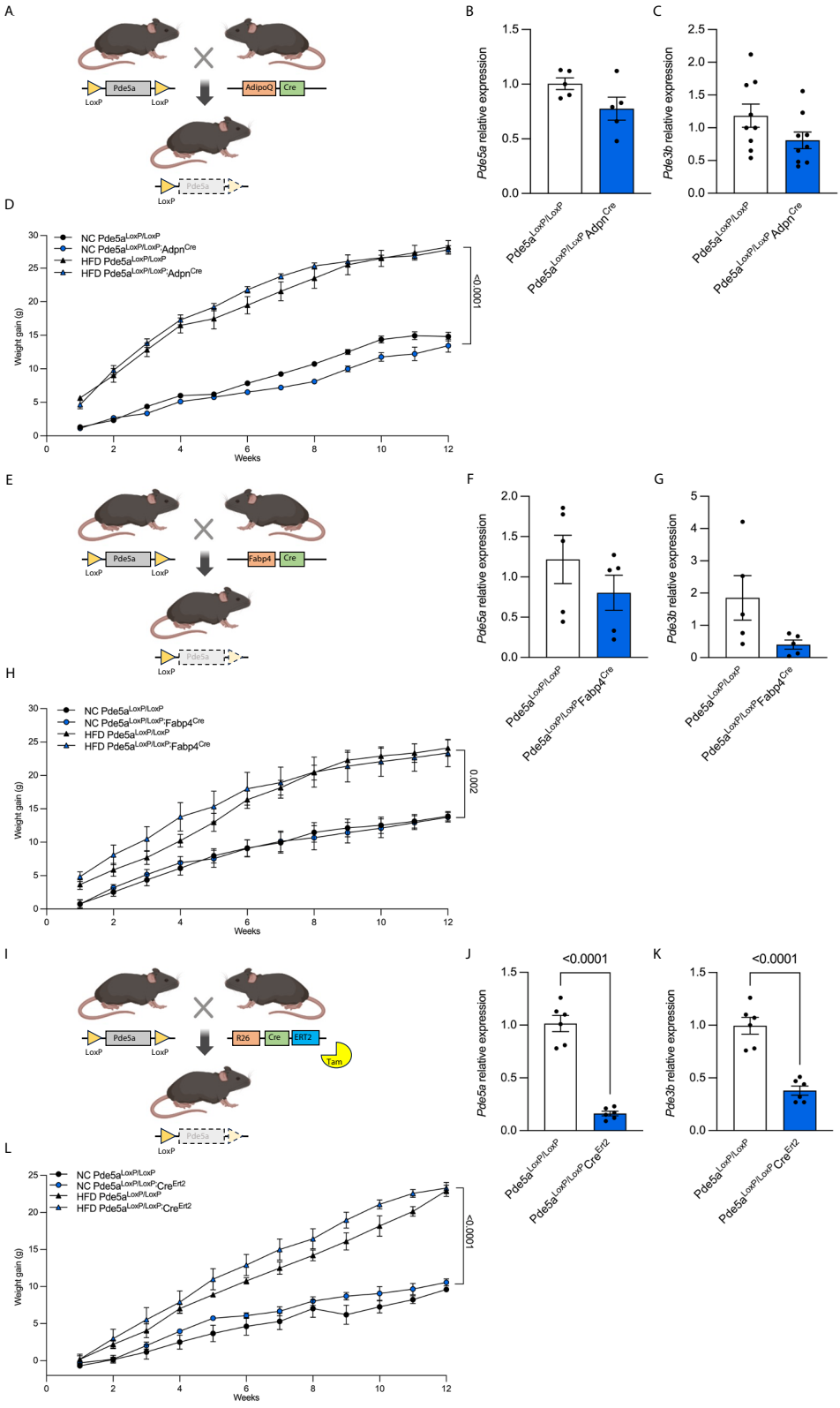

Figure 8: Adipocyte-specific *Pde5a* deletion did not protect mice from HFD-induced obesity. (A) Schematic illustration of targeting strategy for conditional KO of *Pde5a* in mature adipocytes using $Adpn^{Cre}$ mice. **(B-C)** qPCR gene expression analysis of *Pde5a* (B) and *Pde3b* (C) performed on visceral adipose tissue isolated from $Pde5a^{LoxP/LoxP}$ (*white, n = 5*) and *Pde5a* $^{LoxP/LoxP}$; $Adpn^{Cre}$ (*blue, n = 5*). *Hprt1* was used as housekeeping gene for normalization. Data are presented as dot plots with column bars ± SEM. Statistical analysis was performed using Student t-test. **(D)** Relative change in BW (weight gain) of $Pde5a^{LoxP/LoxP}$ (*white*) and *Pde5a* $^{LoxP/LoxP}$*; $Adpn^{Cre}$* (*blue*) fed with HFD or normal chow (NC) over 12 weeks (n = 4 each group). Data are expressed as mean ± SEM. Statistical analysis was performed applying a three-way ANOVA test. **(E)** Schematic illustration of targeting strategy for conditional KO of *Pde5a* in developing adipocytes using $Fabp4^{Cre}$ mice. **(F–G)** qPCR gene expression analysis of *Pde5a* (F) and *Pde3b* (G) performed on

Finally, RNA-seq analysis of liver sample from *Pde5a*$^{-/-}$ identified 477 differentially expressed genes, with 189 genes upregulated and 288 downregulated compared to WT mice. GO analysis revealed that AMPK and insulin signaling pathways, as well as energy metabolism and oxidative phosphorylation processes were strongly induced. Conversely pathways related to insulin resistance, steroid hormone biosynthesis, linoleic acid metabolism and a metabolism signaling were repressed (Figure S4G—I).

In summary, our in-depth and combined analysis of the transcriptome and metabolome confirms *Pde5a*$^{-/-}$ mice undergo substantial metabolomic reprogramming in both adipose tissue and liver, highlighting a global activation of AMPK signaling and a shift in metabolic pathways toward energy expenditure and away from lipid biosynthesis.

4. DISCUSSION

The global prevalence of obesity is rising at an alarming rate, highlighting the urgent need to understand adipose tissue biology to develop effective therapies [2,46]. Increasing evidence suggests that activating BAT and promoting WAT browning are promising strategies to combat obesity [2,23,24]. Preclinical studies investigated the metabolic effects of pharmacological PDE5A inhibition. In particular, Ayala et al. demonstrated that chronic sildenafil treatment enhances insulin sensitivity and promotes a shift toward lipid oxidation in high fat-fed conscious mice, without altering food intake. These beneficial effects were linked to increased oxygen consumption and a reduction in the respiratory exchange ratio, suggesting enhanced mitochondrial fatty acid utilization [10]. Clinical studies have shown that PDE5A inhibition improves lean mass, endothelial function, and insulin sensitivity in humans, supporting the translational relevance of PDE5A targeting for metabolic regulation [47,48]. In this study, we unveil a previously unknown role for PDE5A in energy homeostasis using four distinct *Pde5a* KO mouse models. The first unexpected finding was that the constitutive KO of *Pde5a* does not adversely affect development and reproduction; the mice behave normally and exhibit an unremarkable macroscopic phenotype. However, microscopic analysis reveals significant morphological changes in both white and brown adipose tissue, which turn out to provide robust protection against metabolic challenges. Adipocytes from *Pde5a*$^{-/-}$ mice are significantly smaller and more numerous than WT, due to trans-differentiation of WAT into a more metabolically active adipose tissue, typically triggered by cold exposure or prolonged β-AR stimulation. This trans-differentiation occurs spontaneously in our mouse model, with adipocytes displaying features of *'beige'* adipocytes", such as increased expression of *Ucp1*, mitochondrial activity, and thermogenic potential [18,19]. Under adrenergic or cold stimuli, *Pde5a* KO mice show reduced WAT mass and increased surface temperature, confirming thermogenic activation.

Both browning of adipocytes and BAT hyperactivation confer *Pde5a*$^{-/-}$ mice resistance to liver steatosis, weight gain, and insulin resistance induced by aging or HFD. Metabolomic analysis revealed lower circulating and hepatic lipid levels, both basally and post-challenge corroborated by MRI imaging showing reduced liver fat and enhanced water diffusion. Decreased pro-inflammatory cytokines and a favorable adipokine profile, characterized by increased adiponectin and reduced leptin expression, contribute to a lower adiponectin/leptin ratio, a marker inversely related to liver steatosis and diabetes risk [49,50]. Interestingly, despite the significant reduction in adiposity observed in *Pde5a* deficient mice under HFD, circulating leptin levels remained comparable to those of wild-type controls. Leptin expression is not solely dictated by fat mass but is also influenced by adipocyte function and endocrine signaling dynamics [51]. In our model, the dissociation between fat mass and leptin levels may reflect a reprogrammed adipose tissue state, where endocrine output is recalibrated in the context of enhanced thermogenic capacity and metabolic flexibility. Similar observations have been reported in other models of adipose tissue browning or metabolic remodeling, where leptin levels do not strictly correlate with adiposity or energy balance [52,53]. Moreover, the elevated adiponectin/leptin ratio in *Pde5a* deficient mice supports a metabolically healthier adipose tissue phenotype, despite unchanged leptin levels. Thus, rather than indicating classical leptin resistance, our findings may reflect a shift in the regulatory set point of adipokine secretion in response to early developmental reprogramming.

Despite unchanged food intake and physical activity, *Pde5a*$^{-/-}$ mice exhibit enhanced energy dissipation, favoring heat production over fat accumulation. This mechanism is minimal under basal conditions but activated following metabolic challenges, explaining the absence of body or fat mass differences in resting conditions. During fasting, approximately 80 % of endogenous glucose production comes from liver releases. After a glucose load, insulin suppresses hepatic glucose production and release [54]. Using NMR spectroscopy, we documented an increase in Glucose-1P in *Pde5a*$^{-/-}$ mice, suggesting their liver prioritize glucose as source for glycogen synthesis. Lower lactate and alanine levels, coupled with reduced ^{13}C labeling in glycolytic intermediates and glycerol moieties, further support this shift towards glycogen synthesis over glucose usage. The reduction of liver and circulating triglycerides suggest that *Pde5a* deficient mice rely on alternative energy sources, particularly lipids, under resting conditions. cGMP is emerging as a key regulator of glucose and lipid metabolism [8,9]. While basal cGMP levels in *Pde5a*$^{-/-}$ mice are challenging to detect, increased PKG-dependent phosphorylation of VASP^{Ser239} suggests enhanced cGMP signaling. This affects glucose metabolism by modulating acetyl-CoA carboxylase (ACC), which converts acetyl-CoA into malonyl-CoA, a precursor for de novo lipogenesis [55]; whereas liver ketone bodies synthesis relies on Acetyl-CoA primarily derived from fatty acid oxidation [56]. Consequently, reduced ketone body concentrations in *Pde5a*$^{-/-}$ mice indicate a shift of acetyl-CoA flux towards the TCA cycle rather than hepatic ketogenesis.

RNA-seq confirms upregulation of AMPK signaling in adipose tissue and liver, aligning with its role as a master regulator of lipid metabolism through ACC1 inhibition [57]. Since ACC1 loss promotes browning [58], AMPK activation in *Pde5a*$^{-/-}$ mice likely contributes to

visceral adipose tissue isolated from *Pde5a*$^{LoxP/LoxP}$ (*white,* n = 5) and *Pde5a* $^{LoxP/LoxP}$; *Fabp4*^{Cre} (*blue,* n = 5). *Hprt1* was used as housekeeping gene for normalization. Data are presented as dot plots with column bars ± SEM. Statistical analysis was performed using Student t-test. **(H)** Relative change in BW (weight gain) of *Pde5a*$^{LoxP/LoxP}$ (*white*) and *Pde5a* $^{LoxP/LoxP}$; *Fabp4*^{Cre} *(blue*) fed with HFD or normal chow (NC) over 12 weeks (n = 6 each group). Data are expressed as mean ± SEM. Statistical analysis was performed applying a three-way ANOVA test. **(I)** Schematic illustration of targeting strategy for inducible ubiquitarian conditional KO of *Pde5a* using *Cre*^{Ert2} mice. **(J—K)** qPCR gene expression analysis of *Pde5a* (J) and *Pde3b* (K) performed on visceral adipose tissue isolated from *Pde5a*$^{LoxP/LoxP}$ (*white, n = 5*) and *Pde5a* $^{LoxP/LoxP}$; *Cre*^{Ert2} (*blue, n = 5*). *Hprt1* was used as housekeeping gene for normalization. Data are presented as dot plots with column bars ± SEM. Statistical analysis was performed using Student t-test. **(L)** Relative change in BW (weight gain) of *Pde5a*$^{LoxP/LoxP}$ (*white*) and *Pde5a* $^{LoxP/LoxP}$; *Cre*^{Ert2} (*blue*) fed with HFD or normal chow (NC) over 12 weeks (n = 4 each group). Data are expressed as mean ± SEM. Statistical analysis was performed applying a three-way ANOVA test.

their thermogenic phenotype. Although we did not observe significant differences in ACC transcripts in *Pde5a*$^{-/-}$ mice, supporting evidence also derives from the elevated bile acids (BA) levels found in *Pde5a*$^{-/-}$ mice. BA are known to repress gluconeogenesis, enhance energy expenditure [59], and, via the TGR5 receptor, stimulate liver AMPK [60], endothelial NO-production and cGMP accumulation [61].

Since intracellular cAMP levels in adipose tissue are primarily managed by *Pde3b* [35], we examined its expression and found a significant downregulation, resulting in elevated cAMP levels. Targeted inactivation of *Pde3b* has been shown to enhance cAMP/PKA and AMPK signaling pathways, promoting adipose tissue browning [35,36]. The similarity between the *Pde5a*$^{-/-}$ and *Pde3b*$^{-/-}$ models suggests that the metabolic advantages of *Pde5a* deletion arise from cGMP-cAMP signaling convergence. Studies have demonstrated that increasing cAMP and cGMP levels ameliorates adiposity, upregulates UCP1, and prevents obesity under HFD [52]. *Pde10a* inhibition induces browning of human white adipocytes [62,63], and *Pde4b*$^{-/-}$ mice appear leaner, with lower fat pad weights, smaller adipocytes, and decreased serum leptin levels on both chow and HFD [53]. We uncovered a previously unrecognized interdependency between PDE5 and PDE3 in adipose tissue, demonstrating that *Pde5a* ablation downregulates *Pde3b* via the transcriptional repressor ICER, PDE5A stabilizes PDE3B protein, preventing its degradation and, reciprocally, *Pde3b* silencing suppresses *Pde5a* transcription. Although the metabolic phenotype of *Pde5a* and *Pde3b* KO models appears the same, there are some important differences. First, *Pde3b* ablation induced WAT to beige conversion only in SvJ129 background, whereas in C57BL/6N, a β3-adrenergic stimulation was required to induce WAT browning [64]. Second, the *Pde3b*$^{-/-}$ mice showed signs of insulin resistance, likely due to PGC-1α activation in the liver, whereas PGC-1α was unaffected in *Pde5a*$^{-/-}$ WAT. Finally, *Pde3b*$^{-/-}$ model exhibited increased mitochondrial biogenesis with enlarged mitochondria, while in *Pde5a*$^{-/-}$, mitochondria remained unaffected. Despite heightened cAMP levels, *Pde5a*$^{-/-}$ mice do not exhibit increased lipolysis, suggesting an adaptive response. Indeed, forskolin stimulation fails to induce lipolysis in *Pde5a*$^{-/-}$ adipocytes, suggesting impaired adenylate cyclase activity. *Adcy3*, the primary AC isoform in adipose tissue, is significantly downregulated in *Pde5a*$^{-/-}$ mice, likely as a compensatory mechanism to counteract excessive cAMP signaling and maintain metabolic homeostasis. This explains why *Pde5a* deletion does not induce weight loss under normal feeding conditions. A pivotal role of cGMP in metabolic homeostasis is further supported by *Pde9a* deletion, which enhances BAT activity, increases resting energy expenditure, and mitigates weight gain under HFD [22]. While the metabolic benefits of *Pde9a*$^{-/-}$ and *Pde5a*$^{-/-}$ mice share similarities, the impact of *Pde9a* deletion on the cAMP-PKA axis remains unexplored.

Pde5a is widely distributed across tissues [4], suggesting that the healthy metabolic features observed in *Pde5a* KO mice could be not solely adipocyte-dependent. Indeed, adipocyte-restricted *Pde5a* deletion (achieved using *Adipoq*^{Cre} and *Fabp4*^{Cre} mice) does not replicate the constitutive KO phenotype, implicating a role for other cell populations, presumably within the stromal vascular fraction of AT. Furthermore, inducible post-natal global *Pde5a* deletion (using *Rosa26*^{CreErt2}) fails to confer metabolic protection, suggesting that the observed metabolic reprogramming originates during early development.

The absence of metabolic protection in the conditional *Pde5a* knockout models, despite significant reductions in *Pde5a* and *Pde3b* expression, underscores the importance of developmental timing and critical window during early development in which PDE5A activity may shape long-term metabolic programming. Similar developmental dependencies have been reported in other models of adipose tissue remodeling, where early-life cues are essential for establishing durable metabolic phenotypes [2,40].

Although the overt metabolic phenotype observed in constitutive *Pde5a* KO mice was not recapitulated in conditional KO models, *Pde5a*—*Pde3b* crosstalk remained consistently detectable across all *Pde5a* KO mouse models, underscoring the robustness of this interaction. Collectively, our findings provide a mechanistic framework for targeting PDE5A in metabolic disorders, including the potential modulation of the *Pde5a*—*Pde3b* axis. This therapeutic prospect is further supported by a recent meta-analysis involving over 700 subjects with T2DM, in which prolonged tadalafil (PDE5i) treatment significantly reduced HbA1c levels ($p = 0.002$), with mean treatment effects comparable to established antidiabetic medications suggesting potential clinical relevance [65]. At the same time, our preclinical data help reconcile discrepancies observed in clinical trials, showing that while PDE5 inhibition improves multiple metabolic parameters, it does not necessarily reduce body weight [11,15,65].

5. CONCLUSIONS

This study demonstrates that mice lacking *Pde5a* display a distinctive metabolic phenotype characterized by simultaneous hyperactivation of BAT and induction of beige adipocytes in WAT. This dual thermogenic activation likely underpins the enhanced energy expenditure and resistance to aging and diet-induced obesity observed in these animals. The coordinated recruitment of both brown and beige fat depots suggests a synergistic contribution to thermogenic programming mediated by a previously unrecognized interaction between *Pde5a* and *Pde3b*, which activates cAMP-PKA signaling, driving an early metabolic reprogramming. Our findings position PDE5A as a valuable therapeutic target to enhance thermogenesis, offering a promising adjuvant strategy for combating metabolic disorders.

ACKNOWLEDGMENTS

The authors thank the Euro Bioimaging and the Multi Modal Molecular Imaging Italian Node Facility at the Institute of Biostructures and Bioimaging (CNR) Naples.

The authors thank Dr. Ernesto Soscia for their support in MRI experiments and Dr. Alice Di Stefano and Dr. Tamara Antici for their contributions in IR-thermography experiments.

Parts of Figure 8 and Figure S1 were created using BioRender (https://www.biorender.com).

CRediT AUTHORSHIP CONTRIBUTION STATEMENT

Federica Campolo: Writing — review & editing, Writing — original draft, Visualization, Validation, Resources, Project administration, Methodology, Investigation, Funding acquisition, Formal analysis, Data curation, Conceptualization. **Ottavia Giampaoli:** Writing — review & editing, Writing — original draft, Methodology, Investigation, Formal analysis, Data curation. **Federica Barbagallo:** Formal analysis. **Biagio Palmisano:** Writing — review & editing, Formal analysis. **Anna Di Maio:** Methodology, Investigation, Formal analysis. **Francesca Sciarra:** Formal analysis. **Flavio Rizzo:** Formal analysis. **Serena Monti:** Investigation, Formal analysis. **Sandra Albanese:** Investigation, Formal analysis. **Silvia Cardarelli:** Investigation, Formal analysis. **Maria Rita Assenza:** Investigation, Formal analysis. **Eleonora Poggiogalle:** Writing — review & editing, Methodology, Investigation, Formal analysis, Data curation. **Adriano Patriarca:** Writing —

review & editing, Writing — original draft, Software, Methodology, Investigation, Formal analysis, Data curation. **Fabio Sciubba:** Writing — review & editing, Supervision, Formal analysis, Data curation. **Antonio Filippini:** Resources. **Andrea Lenzi:** Resources. **Daniele Gianfrilli:** Resources. **Mauro Giorgi:** Writing — review & editing, Formal analysis. **Susanna Dolci:** Writing — review & editing, Writing — original draft, Supervision, Resources, Funding acquisition, Formal analysis, Data curation. **Fabio Naro:** Resources. **Maurilio Sampaolesi:** Resources. **Mara Riminucci:** Supervision, Resources. **Alfredo Miccheli:** Writing — review & editing, Writing — original draft, Validation, Supervision, Formal analysis, Data curation. **Lino Tessarollo:** Methodology, Investigation. **Mary Anna Venneri:** Writing — review & editing, Writing — original draft, Supervision, Resources, Funding acquisition. **Andrea M. Isidori:** Writing — review & editing, Writing — original draft, Resources, Funding acquisition.

DECLARATION OF COMPETING INTEREST

Authors have declared that no conflict of interests exists.

FUNDINGS

This work was supported by grants from Italian Ministry of Research (grant no. P2022CE79J to FC; 2020XMLP45_004 to SD) and Sapienza University of Rome (grants no. RM123188F740EABA to FC; AR22117A86D7E9FC to FC; SP122184854B46B6 to FC and RM12218167FC03E8 to MAV). Sapienza University of Rome Research Infrastructures for the HypACB platform for Seahorse experiments is fully acknowledged (grant no. GA116154C8A94E3D).

DATA AVAILABILITY

Data will be made available on request.

APPENDIX A. SUPPLEMENTARY DATA

Supplementary data to this article can be found online at https://doi.org/10.1016/j.molmet.2025.102243.

REFERENCES

[1] Zechner R, Zimmermann R, Eichmann TO, Kohlwein SD, Haemmerle G, Lass A, et al. FAT SIGNALS–lipases and lipolysis in lipid metabolism and signaling. Cell Metab 2012;15:279—91. https://doi.org/10.1016/j.cmet.2011.12.018.

[2] Gesta S, Tseng YH, Kahn CR. Developmental origin of fat: tracking obesity to its source. Cell 2007;131:242—56. https://doi.org/10.1016/j.cell.2007.10.004.

[3] Riazi K, Azhari H, Charette JH, Underwood FE, King JA, Afshar EE, et al. The prevalence and incidence of NAFLD worldwide: a systematic review and meta-analysis. Lancet Gastroenterol Hepatol 2022;7:851—61. https://doi.org/10.1016/S2468-1253(22)00165-0.

[4] Campolo F, Zevini A, Cardarelli S, Monaco L, Barbagallo F, Pellegrini M, et al. Identification of murine phosphodiesterase 5A isoforms and their functional characterization in HL-1 cardiac cell line. J Cell Physiol 2018;233:325—37. https://doi.org/10.1002/jcp.25880.

[5] Li S, Li Y, Xiang L, Dong J, Liu M, Xiang G. Sildenafil induces browning of subcutaneous white adipose tissue in overweight adults. Metabolism 2018;78:106—17. https://doi.org/10.1016/j.metabol.2017.09.008.

[6] Mitschke MM, Hoffmann LS, Gnad T, Scholz D, Kruithoff K, Mayer P, et al. Increased cGMP promotes healthy expansion and browning of white adipose tissue. FASEB J 2013;27:1621—30. https://doi.org/10.1096/fj.12-221580.

[7] Zhang X, Ji J, Yan G, Wu J, Sun X, Shen J, et al. Sildenafil promotes adipogenesis through a PKG pathway. Biochem Biophys Res Commun 2010;396:1054—9. https://doi.org/10.1016/j.bbrc.2010.05.064.

[8] Armani A, Marzolla V, Rosano GM, Fabbri A, Caprio M. Phosphodiesterase type 5 (PDE5) in the adipocyte: a novel player in fat metabolism? Trends Endocrinol Metabol 2011;22:404—11. https://doi.org/10.1016/j.tem.2011.05.004.

[9] Campolo F, Pofi R, Venneri MA, Isidori AM. Priming metabolism with the type 5 phosphodiesterase: the role of cGMP-hydrolyzing enzymes. Curr Opin Pharmacol 2021;60:298—305. https://doi.org/10.1016/j.coph.2021.08.007.

[10] Ayala JE, Bracy DP, Julien BM, Rottman JN, Fueger PT, Wasserman DH. Chronic treatment with sildenafil improves energy balance and insulin action in high fat-fed conscious mice. Diabetes 2007;56(4):1025—33. https://doi.org/10.2337/db06-0883. Apr.

[11] Pofi R, Giannetta E, Feola T, Galea N, Barbagallo F, Campolo F, et al. Sex-specific effects of daily tadalafil on diabetic heart kinetics in RECOGITO, a randomized, double-blind, placebo-controlled trial. Sci Transl Med 2022;14:eabl8503. https://doi.org/10.1126/scitranslmed.abl8503.

[12] West TM, Wang Q, Deng B, Zhang Y, Barbagallo F, Reddy GR, et al. Phosphodiesterase 5 associates with beta2 adrenergic receptor to modulate cardiac function in type 2 diabetic hearts. J Am Heart Assoc 2019;8:e012273. https://doi.org/10.1161/jaha.119.012273.

[13] Venneri MA, Barbagallo F, Fiore D, De Gaetano R, Giannetta E, Sbardella E, et al. PDE5 inhibition stimulates Tie2-expressing monocytes and angiopoietin-1 restoring angiogenic homeostasis in diabetes. J Clin Endocrinol Metab 2019;104:2623—36. https://doi.org/10.1210/jc.2018-02525.

[14] Fiore D, Gianfrilli D, Giannetta E, Galea N, Panio G, di Dato C, et al. PDE5 inhibition ameliorates visceral adiposity targeting the miR-22/SIRT1 pathway: evidence from the CECSID trial. J Clin Endocrinol Metab 2016;101:1525—34. https://doi.org/10.1210/jc.2015-4252.

[15] Giannetta E, Isidori AM, Galea N, Carbone I, Mandosi E, Vizza CD, et al. Chronic Inhibition of cGMP phosphodiesterase 5A improves diabetic cardiomyopathy: a randomized, controlled clinical trial using magnetic resonance imaging with myocardial tagging. Circulation 2012;125:2323—33. https://doi.org/10.1161/circulationaha.111.063412.

[16] Varlamov O, Bethea CL, Roberts Jr CT. Sex-specific differences in lipid and glucose metabolism. Front Endocrinol (Lausanne) 2014;5:241. https://doi.org/10.3389/fendo.2014.00241.

[17] Lopez-Varela S, Sanchez-Muniz FJ, Cuesta C. Decreased food efficiency ratio, growth retardation and changes in liver fatty acid composition in rats consuming thermally oxidized and polymerized sunflower oil used for frying. Food Chem Toxicol 1995;33:181—9. https://doi.org/10.1016/0278-6915(94)00133-9.

[18] Lim S, Honek J, Xue Y, Seki T, Cao Z, Andersson P, et al. Cold-induced activation of brown adipose tissue and adipose angiogenesis in mice. Nat Protoc 2012;7:606—15. https://doi.org/10.1038/nprot.2012.013.

[19] Heine M, Fischer AW, Schlein C, Jung C, Straub LG, Gottschling K, et al. Lipolysis triggers a systemic insulin response essential for efficient energy replenishment of activated brown adipose tissue in mice. Cell Metab 2018;28:644—655 e644. https://doi.org/10.1016/j.cmet.2018.06.020.

[20] Haas B, Mayer P, Jennissen K, Scholz D, Berriel Diaz M, Bloch W, et al. Protein kinase G controls brown fat cell differentiation and mitochondrial biogenesis. Sci Signal 2009;2:ra78. https://doi.org/10.1126/scisignal.2000511.

[21] Moro C, Klimcakova E, Lafontan M, Berlan M, Galitzky J. Phosphodiesterase-5A and neutral endopeptidase activities in human adipocytes do not control

atrial natriuretic peptide-mediated lipolysis. Br J Pharmacol 2007;152:1102–10. https://doi.org/10.1038/sj.bjp.0707485.

[22] Ceddia RP, Liu D, Shi F, Crowder MK, Mishra S, Kass DA, et al. Increased energy expenditure and protection from diet-induced obesity in mice lacking the cGMP-specific phosphodiesterase PDE9. Diabetes 2021;70:2823–36. https://doi.org/10.2337/db21-0100.

[23] Cohen P, Kajimura S. The cellular and functional complexity of thermogenic fat. Nat Rev Mol Cell Biol 2021;22:393–409. https://doi.org/10.1038/s41580-021-00350-0.

[24] Chouchani ET, Kazak L, Spiegelman BM. New advances in adaptive thermogenesis: UCP1 and beyond. Cell Metab 2019;29:27–37. https://doi.org/10.1016/j.cmet.2018.11.002.

[25] Haigh JL, New LE, Filippi BM. Mitochondrial dynamics in the brain are associated with feeding, glucose homeostasis, and whole-body metabolism. Front Endocrinol (Lausanne) 2020;11:580879. https://doi.org/10.3389/fendo.2020.580879.

[26] Gu X, Ma Y, Liu Y, Wan Q. Measurement of mitochondrial respiration in adherent cells by Seahorse XF96 Cell Mito Stress Test. STAR Protoc 2021;2:100245. https://doi.org/10.1016/j.xpro.2020.100245.

[27] Crane JD, Mottillo EP, Farncombe TH, Morrison KM, Steinberg GR. A standardized infrared imaging technique that specifically detects UCP1-mediated thermogenesis in vivo. Mol Metabol 2014;3:490–4. https://doi.org/10.1016/j.molmet.2014.04.007.

[28] Montgomery MK, Hallahan NL, Brown SH, Liu M, Mitchell TW, Cooney GJ, et al. Mouse strain-dependent variation in obesity and glucose homeostasis in response to high-fat feeding. Diabetologia 2013;56:1129–39. https://doi.org/10.1007/s00125-013-2846-8.

[29] Eccleston HB, Andringa KK, Betancourt AM, King AL, Mantena SK, Swain TM, et al. Chronic exposure to a high-fat diet induces hepatic steatosis, impairs nitric oxide bioavailability, and modifies the mitochondrial proteome in mice. Antioxidants Redox Signal 2011;15:447–59. https://doi.org/10.1089/ars.2010.3395.

[30] Sun Y, Ge X, Li X, He J, Wei X, Du J, et al. High-fat diet promotes renal injury by inducing oxidative stress and mitochondrial dysfunction. Cell Death Dis 2020;11:914. https://doi.org/10.1038/s41419-020-03122-4.

[31] Kim J, Oh CM, Kim H. The interplay of adipokines and pancreatic beta cells in metabolic regulation and diabetes. Biomedicines 2023;11. https://doi.org/10.3390/biomedicines11092589.

[32] Tilg H, Moschen AR. Adipocytokines: mediators linking adipose tissue, inflammation and immunity. Nat Rev Immunol 2006;6:772–83. https://doi.org/10.1038/nri1937.

[33] Seo DH, Shin E, Lee YH, Park SE, Nam KT, Kim JW, et al. Effects of a phosphodiesterase inhibitor on the browning of adipose tissue in mice. Biomedicines 2022;10. https://doi.org/10.3390/biomedicines10081852.

[34] Reinhardt RR, Chin E, Zhou J, Taira M, Murata T, Manganiello VC, et al. Distinctive anatomical patterns of gene expression for cGMP-inhibited cyclic nucleotide phosphodiesterases. J Clin Investig 1995;95:1528–38. https://doi.org/10.1172/jci117825.

[35] Choi YH, Park S, Hockman S, Zmuda-Trzebiatowska E, Svennelid F, Haluzik M, et al. Alterations in regulation of energy homeostasis in cyclic nucleotide phosphodiesterase 3B-null mice. J Clin Investig 2006;116:3240–51. https://doi.org/10.1172/jci24867.

[36] Chung YW, Ahmad F, Tang Y, Hockman SC, Kee HJ, Berger K, et al. White to beige conversion in PDE3B KO adipose tissue through activation of AMPK signaling and mitochondrial function. Sci Rep 2017;7:40445. https://doi.org/10.1038/srep40445.

[37] Honnor RC, Dhillon GS, Londos C. cAMP-dependent protein kinase and lipolysis in rat adipocytes. II. Definition of steady-state relationship with lipolytic and antilipolytic modulators. J Biol Chem 1985;260:15130–8. https://doi.org/10.1016/S0021-9258(18)95712-1.

[38] Djouder N, Tuerk RD, Suter M, Salvioni P, Thali RF, Scholz R, et al. PKA phosphorylates and inactivates AMPKalpha to promote efficient lipolysis. EMBO J 2010;29:469–81. https://doi.org/10.1038/emboj.2009.339.

[39] Allen MD, Zhang J. Subcellular dynamics of protein kinase A activity visualized by FRET-based reporters. Biochem Biophys Res Commun 2006;348:716–21. https://doi.org/10.1016/j.bbrc.2006.07.136.

[40] Eguchi J, Wang X, Yu S, Kershaw EE, Chiu PC, Dushay J, et al. Transcriptional control of adipose lipid handling by IRF4. Cell Metab 2011;13:249–59. https://doi.org/10.1016/j.cmet.2011.02.005.

[41] Palmisano B, Labella R, Donsante S, Remoli C, Spica E, Coletta I, et al. Gsalpha(R201C) and estrogen reveal different subsets of bone marrow adiponectin expressing osteogenic cells. Bone Res 2022;10:50. https://doi.org/10.1038/s41413-022-00220-1.

[42] Zhu B, Strada S, Stevens T. Cyclic GMP-specific phosphodiesterase 5 regulates growth and apoptosis in pulmonary endothelial cells. Am J Physiol Lung Cell Mol Physiol 2005;289:L196–206. https://doi.org/10.1152/ajplung.00433.2004.

[43] Gebska MA, Stevenson BK, Hemnes AR, Bivalacqua TJ, Haile A, Hesketh GG, et al. Phosphodiesterase-5A (PDE5A) is localized to the endothelial caveolae and modulates NOS3 activity. Cardiovasc Res 2011;90:353–63. https://doi.org/10.1093/cvr/cvq410.

[44] Jeffery E, Berry R, Church CD, Yu S, Shook BA, Horsley V, et al. Characterization of Cre recombinase models for the study of adipose tissue. Adipocyte 2014;3:206–11. https://doi.org/10.4161/adip.29674.

[45] Dastagir K, Reimers K, Lazaridis A, Jahn S, Maurer V, Strauss S, et al. Murine embryonic fibroblast cell lines differentiate into three mesenchymal lineages to different extents: new models to investigate differentiation processes. Cell Reprogr 2014;16:241–52. https://doi.org/10.1089/cell.2014.0005.

[46] Kim MS, Shim I, Fahed AC, Do R, Park WY, Natarajan P, et al. Association of genetic risk, lifestyle, and their interaction with obesity and obesity-related morbidities. Cell Metab 2024;36:1494–1503 e1493. https://doi.org/10.1016/j.cmet.2024.06.004.

[47] Aversa A, Fittipaldi S, Francomano D, Bimonte VM, Greco EA, Crescioli C, et al. Tadalafil improves lean mass and endothelial function in nonobese men with mild ED/LUTS: in vivo and in vitro characterization. Endocrine 2017;56:639–48. https://doi.org/10.1007/s12020-016-1208-y.

[48] Maneschi E, Cellai I, Aversa A, Mello T, Filippi S, Comeglio P, et al. Tadalafil reduces visceral adipose tissue accumulation by promoting preadipocytes differentiation towards a metabolically healthy phenotype: studies in rabbits. Mol Cell Endocrinol 2016;424:50–70. https://doi.org/10.1016/j.mce.2016.01.015.

[49] Joseph JJ, Kluwe B, Echouffo-Tcheugui JB, Zhao S, Brock G, Kline D, et al. Association of adiposity with incident diabetes among black adults in the jackson heart study. J Am Heart Assoc 2021;10:e020716. https://doi.org/10.1161/jaha.120.020716.

[50] Nedungadi D, Adesanya TMA, Rayan MN, Zhao S, Williams A, Brock G, et al. The association of adiposity and RAAS with incident diabetes in African Americans: the Jackson heart study. J Clin Endocrinol Metab 2024. https://doi.org/10.1210/clinem/dgae396.

[51] Caron A, Lee S, Elmquist JK, Gautron L. Leptin and brain-adipose crosstalks. Nat Rev Neurosci 2018;19(3):153–65. https://doi.org/10.1038/nrn.2018.7. Feb 16.

[52] Kim NJ, Baek JH, Lee J, Kim H, Song JK, Chun KH. A PDE1 inhibitor reduces adipogenesis in mice via regulation of lipolysis and adipogenic cell signaling. Exp Mol Med 2019;51:1–15. https://doi.org/10.1038/s12276-018-0198-7.

[53] Zhang R, Maratos-Flier E, Flier JS. Reduced adiposity and high-fat diet-induced adipose inflammation in mice deficient for phosphodiesterase 4B. Endocrinology 2009;150:3076–82. https://doi.org/10.1210/en.2009-0108.

[54] Kowalski GM, Bruce CR. The regulation of glucose metabolism: implications and considerations for the assessment of glucose homeostasis in rodents. Am

J Physiol Endocrinol Metab 2014;307:E859—71. https://doi.org/10.1152/ajpendo.00165.2014.

[55] Garcia-Villafranca J, Guillen A, Castro J. Involvement of nitric oxide/cyclic GMP signaling pathway in the regulation of fatty acid metabolism in rat hepatocytes. Biochem Pharmacol 2003;65:807—12. https://doi.org/10.1016/s0006-2952(02)01623-4.

[56] McGarry JD, Foster DW. Regulation of hepatic fatty acid oxidation and ketone body production. Annu Rev Biochem 1980;49:395—420. https://doi.org/10.1146/annurev.bi.49.070180.002143.

[57] Li Y, Xu S, Mihaylova MM, Zheng B, Hou X, Jiang B, et al. AMPK phosphorylates and inhibits SREBP activity to attenuate hepatic steatosis and atherosclerosis in diet-induced insulin-resistant mice. Cell Metab 2011;13:376—88. https://doi.org/10.1016/j.cmet.2011.03.009.

[58] Guilherme A, Rowland LA, Wetoska N, Tsagkaraki E, Santos KB, Bedard AH, et al. Acetyl-CoA carboxylase 1 is a suppressor of the adipocyte thermogenic program. Cell Rep 2023;42:112488. https://doi.org/10.1016/j.celrep.2023.112488.

[59] Zhang X, Yang S, Chen J, Su Z. Unraveling the regulation of hepatic gluconeogenesis. Front Endocrinol (Lausanne) 2018;9:802. https://doi.org/10.3389/fendo.2018.00802.

[60] Watanabe M, Houten SM, Mataki C, Christoffolete MA, Kim BW, Sato H, et al. Bile acids induce energy expenditure by promoting intracellular thyroid hormone activation. Nature 2006;439:484—9. https://doi.org/10.1038/nature04330.

[61] Kida T, Tsubosaka Y, Hori M, Ozaki H, Murata T. Bile acid receptor TGR5 agonism induces NO production and reduces monocyte adhesion in vascular endothelial cells. Arterioscler Thromb Vasc Biol 2013;33:1663—9. https://doi.org/10.1161/atvbaha.113.301565.

[62] Hankir MK, Kranz M, Gnad T, Weiner J, Wagner S, Deuther-Conrad W, et al. A novel thermoregulatory role for PDE10A in mouse and human adipocytes. EMBO Mol Med 2016;8:796—812. https://doi.org/10.15252/emmm.201506085.

[63] Tomaszewski MR, Meng X, Haley HD, Harrell CM, McDonald TP, Miller CO, et al. Magnetic resonance imaging detects white adipose tissue beigeing in mice following PDE10A inhibitor treatment. J Lipid Res 2023;64:100408. https://doi.org/10.1016/j.jlr.2023.100408.

[64] Guirguis E, Hockman S, Chung YW, Ahmad F, Gavrilova O, Raghavachari N, et al. A role for phosphodiesterase 3B in acquisition of brown fat characteristics by white adipose tissue in male mice. Endocrinology 2013;154:3152—67. https://doi.org/10.1210/en.2012-2185.

[65] Fryk E, Rodrigues Silva VR, Bauza-Thorbrugge M, Schmelz M, Gan LM, Strindberg L, et al. Feasibility of high-dose tadalafil and effects on insulin resistance in well-controlled patients with type 2 diabetes (MAKROTAD): a single-centre, double-blind, randomised, placebo-controlled, cross-over phase 2 trial. eClinicalMedicine 2023;59:101985. https://doi.org/10.1016/j.eclinm.2023.101985.

